Czech Technical University in Prague
Faculty of Civil Engineering

The Department of Landscape Water Conservation
Environmental Engineering

Diploma Thesis

Modeling of Water Flow and Nutrient Transport in Green Roofs

Bc. Razbar Wahab

Study program: Water and Environmental Engineering
Specialization: Environmental Engineering and Science
Supervisor: doc. Ing. Michal Sněhota, Ph.D.

Prague, 2024

MASTER‘S THESIS ASSIGNMENT

I. Personal and study details

Student's name: **Wahab Razbar** Personal ID number: **517012**

Faculty / Institute: **Faculty of Civil Engineering**

Department / Institute: **Department of Landscape Water Conservation**

Study program: **Water and Environmental Engineering**

Specialisation: **Environmental Engineering and Science**

II. Master’s thesis details

Master’s thesis title in English:

Modeling of water flow and nutrient transport in green roof

Master’s thesis title in Czech:

Modeling of water flow and nutrient transport in green roof

Guidelines:

The objective of this thesis is to model the flow and nutrient transport in a hybrid green roof system consisting of a constructed wetland and an extensive green roof. This study will conduct a comprehensive literature review on the state of the art of green roof and constructed wetland modeling. In the practical part, the student will re-assess the archived data from earlier experiment conducted on small hybrid green roof testbed (Petreje et al., 2023). The conceptual model will be developed. Then, numerical modeling of water flow, conservative tracer and nutrients in the hybrid green roof system will be performed for selected events using HYDRUS 2D. Optionally, the numerical experiments will be performed for higher nutrient loads. The expected results of this study are a digital representation of the h ybrid green roof system that can lead to a better understanding and design.

Bibliography / sources:

Articles listed in Web of Science
Petreje, M., Sněhota, M., Chorazy, T., Novotný, M., Rybová, B., Hečková, P., 2023. Performance study of an innovative concept of hybrid constructed wetland-extensive green roof with growing media amended with recycled materials. Journal of Environmental Management 331, 117151. https://doi.org/10.1016/j.jenvman.2022.117151

Name and workplace of master’s thesis supervisor:

doc. Ing. Michal Sněhota, Ph.D. Department of Landscape Water Conservation FCE

Name and workplace of second master’s thesis supervisor or consultant:

Date of master’s thesis assignment: **19.02.2024** Deadline for master's thesis submission: **20.05.2024**

Assignment valid until: _____

doc. Ing. Michal Sněhota, Ph.D.	prof. Dr. Ing. Tomáš Dostál	prof. Ing. Jiří Máca, CSc.
Supervisor’s signature	Head of department’s signature	Dean’s signature

III. Assignment receipt

The student acknowledges that the master’s thesis is an individual work. The student must produce her thesis without the assistance of others, with the exception of provided consultations. Within the master’s thesis, the author must state the names of consultants and include a list of references.

.	
Date of assignment receipt	Student’s signature

DECLARATION

I declare that I have prepared my thesis independently under the supervision of doc. Ing. Michal Sněhota, Ph.D. and with the help of the mentioned sources of information.

Prague, 21.5.2024 ……

Razbar Wahab

ACKNOWLEDGEMENTS

I would like to thank my thesis supervisor, doc. Ing. Michal Sněhota, Ph.D., for his exceptional guidance, patience, and unwavering support throughout this project. His enthusiasm has been a constant source of motivation, inspiring me to work harder and explore the depths of this research with greater dedication. I would also like to extend my heartfelt thanks to PhD student Marek Petreje for his invaluable help.

I am deeply grateful to my husband, Lawen, for his constant support and encouragement throughout this journey, my mother for her unconditional love, and endless sacrifices, and my sister, Zna, for always being there for me.

ABSTRACT

This thesis investigates the modeling of water flow and solute transport within a hybrid green roof system incorporating a constructed wetland and a semi-intensive green roof. Utilizing HYDRUS-2D software, simulations were performed to evaluate the performance and dynamics of this integrated system and build a digital twin that can replicate the experiment. Modeled pressure heads demonstrated increases during irrigation pulses and rainfall events, particularly near the surface, reflecting effective infiltration and redistribution of water. Simulations of solute transport and fate related to BOD_5 demonstrated the system's ability to reduce solute concentration. The results showed a marked decrease in BOD_5 levels near the outlet, highlighting the green roof's effectiveness in degrading organic matter.

These results contribute to a deeper understanding of recently developed hybrid, constructed wetland-green roof system, offering insights into optimizing its design and operational strategies for its enhanced water management and environmental benefits. The research emphasizes the potential of hybrid green roofs to improve urban sustainability through effective water and solute management.

Keywords:

Green roofs, constructed wetlands, modeling of water flow, HYDRUS-2D

ABSTRAKT

Tato práce se zabývá modelováním proudění vody a transportu rozpuštěných látek v rámci hybridního systému zelených střech zahrnujícího umělý mokřad a polointenzivní zelenou střechu. S využitím softwaru HYDRUS-2D byly provedeny simulace za účelem vyhodnocení výkonnosti a dynamiky tohoto integrovaného systému a vytvoření digitálního dvojčete, které dokáže simulovat experiment. Modelované tlakové výšky vykazovaly nárůst během zavlažovacích pulzů a dešťových událostí, zejména v blízkosti povrchu, což odráží účinnou infiltraci a redistribuci vody. Simulace transportu a osudu rozpuštěných látek v souvislosti s BSK5 prokázaly schopnost systému snižovat koncentraci rozpuštěných látek. Výsledky ukázaly výrazný pokles hladin BSK5 v blízkosti odtoku, což zdůrazňuje účinnost zelené střechy při rozkladu organických látek.

Tyto výsledky přispívají k hlubšímu pochopení nedávno vyvinutého hybridního systému umělého mokřadu a zelené střechy a nabízejí poznatky o optimalizaci jeho konstrukčních a provozních strategií pro lepší hospodaření s vodou a přínosy pro životní prostředí. Výzkum zdůrazňuje potenciál hybridních zelených střech pro zlepšení udržitelnosti měst prostřednictvím účinného hospodaření s vodou a rozpuštěnými látkami.

Keywords:

Green roofs, Constructed wetlands, modeling of water flow, HYDRUS-2D

TABLE OF CONTENTS

1. INTRODUCTION

1.1. Introduction to Environmental challenges and Water Scarcity

Climate change represents one of the most pressing global challenges of our time. Temperatures rising, altered weather patterns, and increasingly extreme weather events are some of the significant climate shifts. Shifts in precipitation patterns lead to droughts in some regions and increased precipitation and flooding in others, disrupting agriculture, water resources, and livelihoods (Calvin et al., 2023)

Along with climate change, population growth, rapid urbanization and poor water management are factors causing water demand to outpace its availability in many regions around the world, thus leading to water scarcity. Not only does water scarcity impact ecosystems but also raises concerns about humans' well-being, food security, and economies and therefore must be addressed through effective water management strategies and conservation efforts (Liu et al., 2017).

1.2. Green Roofs and Concept of wastewater reuse

Green roofs are widely used to contribute to environmental improvement as they offer various benefits including stormwater mitigation, decreasing cooling demands of buildings, biodiversity conservation, and visual aesthetics (Getter & Rowe, 2006). A sustainable practice in managing green roofs is use of treated greywater for irrigation, decreasing the demand for fresh water. Greywater is wastewater excluding toilet waste and can be treated on site using different technologies such as constructed wetlands, biofilters, and membrane reactors.

1.3. Numerical modelling

Numerical modelling of the unsaturated zone plays a crucial role in understanding and predicting various processes occurring in the subsurface such as fluid flow, solute transport, and irrigation event (Kollet & Maxwell, 2006). By simulating complex scenarios that may be difficult to observe directly, these models help scientists visualize and better understand these processes. This leads to better understanding of the subsurface and the vadose zone, which can result in improved management and planning. Numerical models are also capable of approximating the solutions of equations that are difficult to solve directly, making them a valuable tool for subsurface analysis.

2. OBJECTIVE AND STRUCTURE OF THE THESIS

This thesis aims to contribute to a comprehensive understanding of the mechanisms involved in using novel concept of hybrid green roof that consists of constructed wetland and semi extensive green roofs parts. Specifically, I aim to construct a mathematical model using HYDRUS-2D to simulate water flow and nutrient transport within a constructed wetland and green roof system based on an experiment conducted in Brno, Czech Republic (Petreje et al., 2023). The structure of the thesis encompasses seven chapters: a thorough literature review to contextualize the research, a detailed methodology section outlining the modeling approach for water flow and nutrient transport, presentation of results obtained from the experiments and simulations, and discussions to interpret findings, address limitations, and propose future research directions. Through this structured approach, the thesis aims to contribute to the advancement of sustainable water management practices and the utilization of green infrastructure for environmental conservation.

3. LITERATURE REVIEW

The first part of this diploma thesis focuses on research of published literature on topics of constructed wetlands, green roofs, and water flow modelling, specifically using HYDRUS software.

3.1. Green Roofs

A green roof is a type of roof that is covered with vegetation and a growing medium, providing a range of ecosystem services in urban areas. These services include improved storm-water management, regulation of building temperatures and reduction of urban heat-island effects (Oberndorfer et al., 2007). Green roofs also offer economic benefits to the public and farmers, while reducing CO_2 emissions and providing habitat for wildlife (Li & Babcock, 2014).

3.1.1. Types of Green Roofs

Green roofs can be intensive or extensive. Intensive green roofs have historically been implemented with deep substrates and resemble ground level gardens. On the other hand, extensive green roofs are a more modern modification of green roofs with shallower substrates and overall lower maintenance requirements (Oberndorfer et al., 2007). Table 1 shows a comparison of properties of each type.

Table 1 A comparison of extensive and intensive green roofs (Oberndorfer et al., 2007)

Characteristic	Extensive Roof	Intensive Roof
Purpose	Functional; storm-water management, thermal insulation, fireproofing	Functional and aesthetic; increased living space
Structural Requirements	Typically within standard roof weight-bearing parameters; additional 70 to 170 kg per m² (Dunnet and Kingsbury 2004)	Planning required in design phase or structural improvements necessary; additional 290 to 970 kg per m²
Substrate Type	Lightweight; high porosity, low organic matter	Lightweight to heavy; high porosity, low organic matter
Average Substrate Depth	2 to 20 cm	20 cm or more
Plant Communities	Low-growing communities of plants and mosses selected for stress-tolerance qualities (e.g., Sedum spp., Sempervivum spp.)	No restrictions other than those imposed by substrate depth, climate, building height, exposure, and irrigation facilities
Irrigation	Most require little or no irrigation	Often require irrigation
Maintenance	Little or no maintenance required; some weeding or moving as necessary	Same maintenance requirements as a similar garden at ground level
Accessibility	Generally functional rather than accessible; will need basic accessibility for maintenance	Typically accessible; bylaw considerations

3.1.2. Green Roof Components

The major components of a green roof typically include several layers that work together to create a functional and sustainable system. These layers are designed carefully to support vegetation growth and provide the ecosystem services. Common components of a green roof system are shown in Figure 1. Most green roofs share common construction elements. A root barrier is positioned over the standard roofing membrane to safeguard against root penetration damage. Positioned above the root barrier is a drainage layer, facilitating the removal of excess water from the roof. Atop the drainage layer sits a filter fabric, which prevents silt and particulate matter within the media from obstructing the drainage layer. Optionally, a water retention fabric may be placed over this layer, with water retention being influenced by design considerations like substrate depth, composition, and plant varieties, as well as environmental factors such as rainfall intensity and duration (Getter & Rowe, 2006).

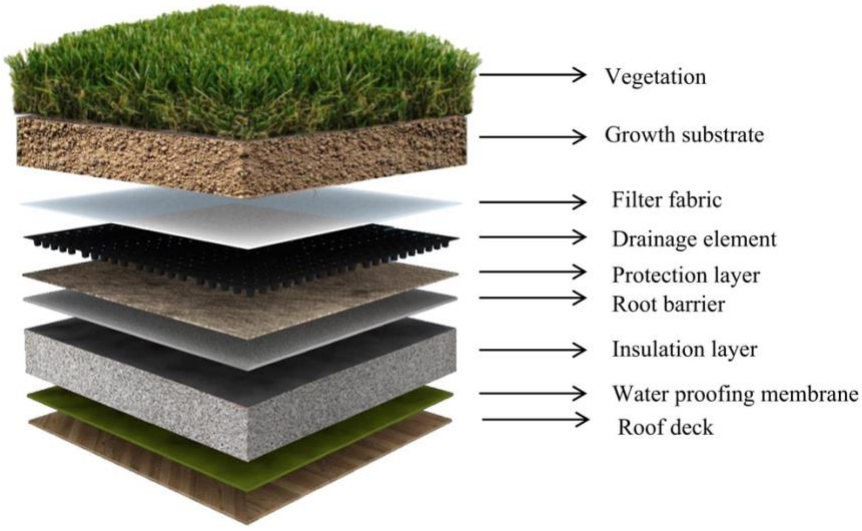

Figure 1 Components of a green roof, adapted from Vijayaraghavan (2016)

Growing media

The growing media of green roofs play a crucial role in supporting vegetation and facilitating the ecological functions of these systems. Careful selection of substrates for green roofs growing media is very important as various factors must be considered, as the green roof system directly impacts the structural integrity of the building. Composed of a blend of materials, green roof substrates must keep a balance between providing necessary support for plant growth, ensuring efficient water drainage, and minimizing weight loads on the building

structure (Lata et al., 2018). Typically, green roof substrates consist of a mix of lightweight, well-drained mineral-based materials such as expanded slate, shale, or clay, supplemented by inorganic components like sand, pumice, perlite, and vermiculite (Getter & Rowe, 2006). These materials offer sufficient pore space for water retention and root growth while promoting proper aeration within the substrate. Additionally, the composition of the growing media is tailored to meet specific design requirements, including substrate depth, composition, and plant species selection.

A study by (Wang et al., 2017) examines the effectiveness of dual-substrate-layer extensive green roofs in rainwater retention and pollutant reduction, comparing them with traditional single-substrate-layer roofs. Dual-substrate-layer roofs, comprising an organic layer for plant growth and an inorganic layer for water retention and pollutant reduction, supported superior vegetation growth compared to single-substrate-layer roofs. Utilizing a mixture of activated charcoal, perlite, and vermiculite as the adsorption substrate, dual-substrate-layer roofs exhibited better rainfall retention performance. They acted as sinks for organics, heavy metals, and nitrogen forms but as sources of phosphorus contaminants during heavy rains. A combination of activated charcoal and/or pumice with perlite and vermiculite is recommended for optimal water retention and pollution reduction.

3.2. Constructed Wetlands

3.2.1. Principles and Applications

Constructed wetlands are engineered systems that use natural materials and processes to treat water and wastewater, providing a cost-effective and environmentally friendly alternative to conventional treatment methods (A. Stefanakis, 2016). They are effective in removing a wide range of contaminants and can be used for domestic, municipal, and industrial wastewater treatment, as well as sludge dewatering and drying (A. Stefanakis, 2016). In addition to their primary function of water purification, constructed wetlands also provide ancillary benefits such as creating natural habitats, supporting wildlife, and offering recreational and cultural opportunities (Ghermandi, 2005).

According to (Kadlec et al., 2000), constructed wetlands can be classified into two main types based on water flow: free water surface (FWS) and subsurface flow (SSF) wetlands. FWS wetlands are characterized by shallow basins or channels with emergent vegetation. In contrast, SSF wetlands consist of a bed of porous media with vegetation and can be further divided into horizontal flow and vertical flow systems. Figure 2 presents schematic representations of four

types of constructed wetlands as adapted from (A. Stefanakis, 2016): free water surface constructed wetlands, horizontal subsurface flow constructed wetlands, vertical subsurface flow constructed wetlands, and floating wetlands. Additionally, constructed wetlands can be categorized by the type of vegetation they support. According to (Vymazal, 2007), these categories include emergent macrophyte wetlands, submerged macrophyte wetlands, and floating treatment wetlands.

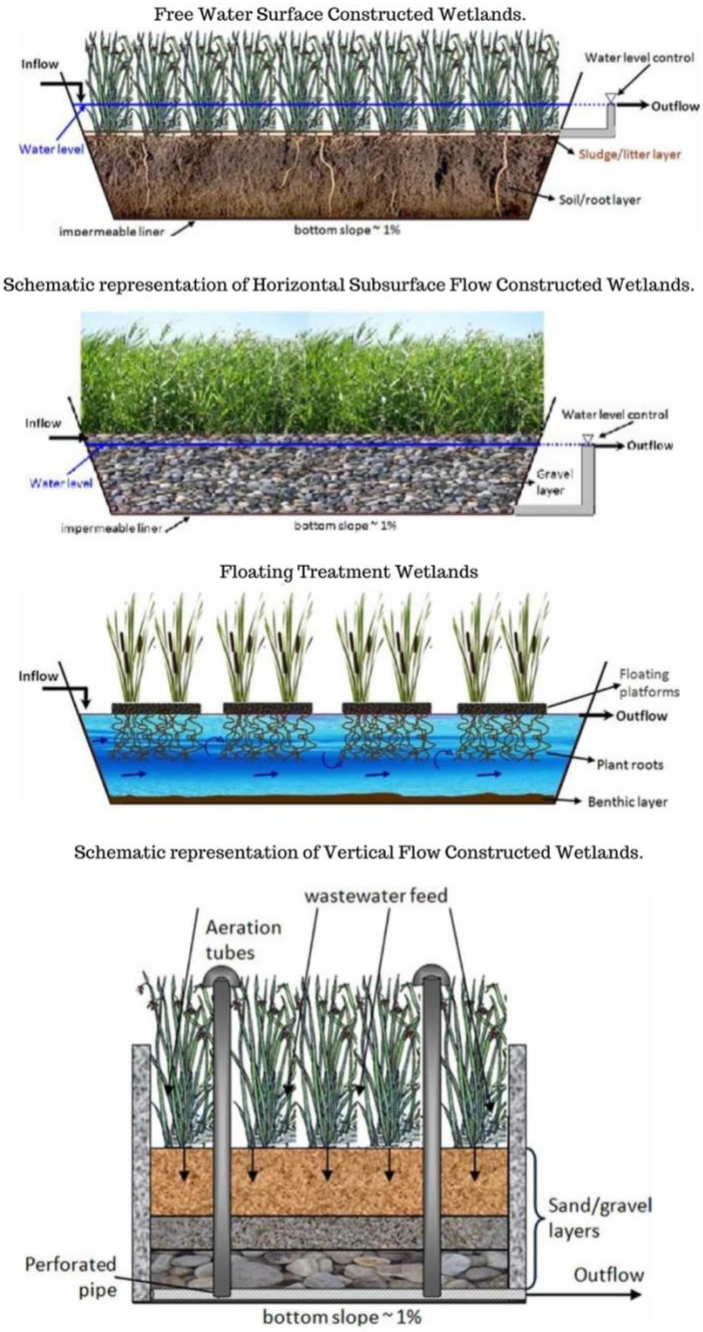

Figure 2 Four types of constructed wetlands, adapted from (A. Stefanakis, 2016)

3.2.2. Constructed Wetlands in Combination with Green Roofs

Green roofs and constructed wetlands as two elements of blue-green infrastructure can be combined to create a hybrid system. Green roofs mimic natural ecosystems and provide ecosystem services, such as stormwater management and habitat provision (Oberndorfer et al., 2007) On the other hand, constructed wetlands are established green infrastructure solutions for water management and wastewater treatment, offering environmental and economic benefits (A. I. Stefanakis, 2019).

Combining these two elements has the potential to boost water treatment capabilities and offer added environmental advantages. The utilization of decentralized eco-technologies in water management, such as green roofs and constructed wetlands, is seen as a promising approach. This integration not only has the capacity to enhance urban biodiversity but also to mitigate the adverse impacts of isolation and fragmentation on biodiversity. In a study by (Knapp et al., 2019), it was noted that the combined use of green roofs and constructed wetlands could help achieve these goals. In another study by (Petreje et al., 2023), the effectiveness of horizontally flowing constructed wetlands in removing nutrients from greywater was demonstrated through chemical analysis, water temperature observations, water balance assessments, and other monitoring techniques. The research found that the constructed wetland significantly reduced concentrations of total nitrogen and orthophosphate in pre-treated greywater. Furthermore, the study shows that the concept of incorporating recycled materials into novel growing media for hybrid roofs adds another dimension to this approach.

3.3. Greywater

Municipal sewage is primarily divided into yellow, brown, and greywater based on the presence or absence of urine and fecal sewage with greywater being the most suitable for reuse due to its large volume and relatively low concentration of pollutants (DeOreo et al., 2016). Greywater (GW) refers to household wastewater that does not include toilet waste, encompassing water from activities such as laundry, handwashing, washing machines, dishwashing, showers, and kitchen sinks (Maimon et al., 2010). The reuse of greywater can help meet populations' demand for freshwater, as the reused greywater can be used for irrigation, domestic uses, or other non-potable purposes (Chu et al., 2004) and is generated at a high volume in domestic properties, constituting around 50 to 70% of the total daily water discharge (Moslemi Zadeh et al., 2013). A scheme of greywater generation and reuse possibilities is presented in Figure 3. According to (Revitt et al., 2011) it is estimated that

greywater recycling could result in potable water savings of up to 43%, based on Danish water use data and monitoring of priority substances at a greywater treatment facility in Denmark. Greywater is often divided into two categories based on contaminant levels: light greywater (LGW) and dark greywater (DGW). LGW comes from baths, showers, hand basins, and bathroom sinks, while DGW comes from laundry, washing machines, kitchens, and dishwashers. LGW has fewer contaminants than DGW. Mixed greywater includes both LGW and DGW sources (Alsulaili & Hamoda, 2015).

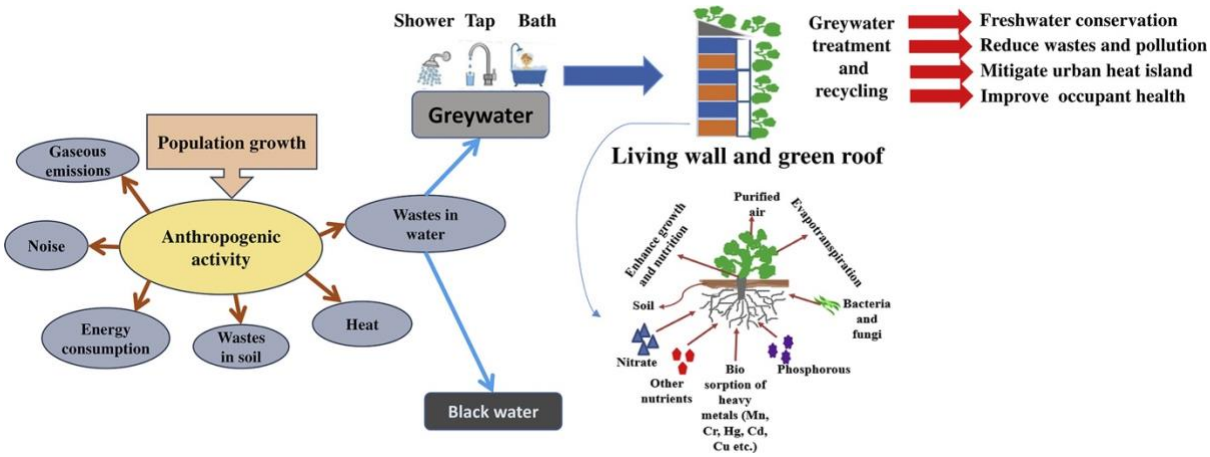

Figure 3 Greywater Generation and Reuse, adapted from (Pradhan et al., 2019)

A review article by (Albalawneh & Chang, 2015) found that the amount of greywater generated ranges from 90 to 120 liters per person per day, though in low-income nations facing persistent water scarcity, this figure can drop to as little as 20–30 liters per person per day. The authors also found and plotted that differences in greywater volume are also evident between urban and rural regions, as seen in Figure 4.

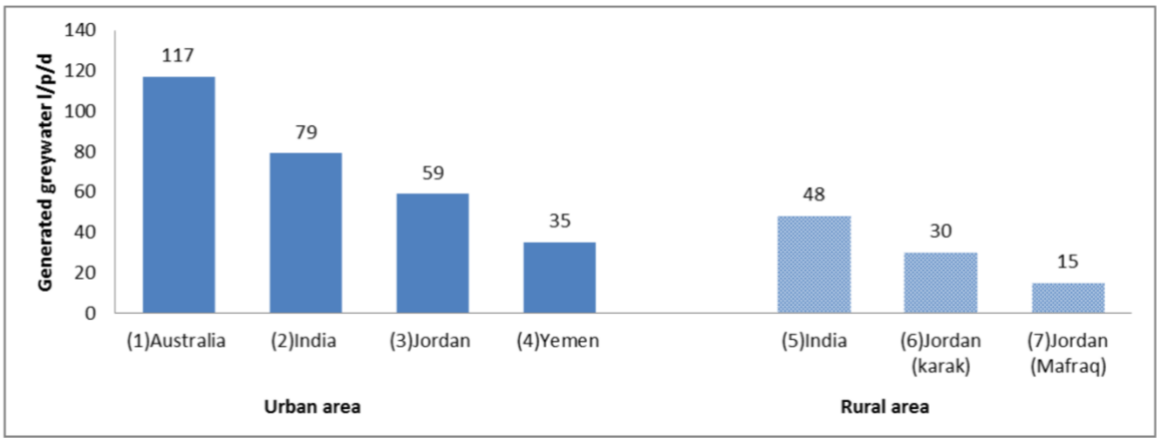

Figure 4 The volume of greywater generated in urban versus rural areas, adapted from (Albalawneh & Chang, 2015)

3.3.1. Chemical characteristics of greywater

Greywater quality and composition fluctuate depending on its source and the contaminants it contains, often originating from chemicals present in the water source (Revitt et al., 2011). Compared to mixed sewage water, greywater typically contains higher concentrations of metals due to the presence of personal care products, cleaning agents, and dyes, leading to elevated levels of heavy metals, chlorine, and total organic carbon. Greywater is typically characterized by its high nutrient content, particularly phosphorus and nitrogen (Shaikh & Ahammed, 2020). According to a review by (Shaikh & Ahammed, 2020) of numerous studies, dark greywater has the highest pH, while bathroom effluents have the lowest pH. Kitchen effluents have the highest biological oxygen demand (BOD), and light greywater has the lowest. Dark greywater has the highest chemical oxygen demand (COD), and hand basin effluents have the lowest. Bathroom effluents have the highest total nitrogen content, and kitchen effluents have the lowest. Kitchen effluents have the highest total phosphates, and hand basins have the lowest. Table. 2 shows a comparison of the chemical characteristics from different sources.

Table 2 Chemical characteristics of greywater from different sources, Adapted from (Shaikh & Ahammed, 2020)

Parameter	Bathroom	Hand Basin	Kitchen	Laundry	Light Greywater	Dark Greywater
pH	5.94–8.40 (35)	6.72–9.82 (11)	5.58–10.00 (14)	5.00–10.33 (20)	4.90–8.53 (63)	5.00–10.33 (34)
BOD (mg/L)	20–673 (35)	33–305 (12)	185–2460 (10)	44–3330 (17)	20–673 (64)	44–3330 (29)
COD (mg/L)	64–903 (38)	47–587 (14)	411–8071 (9)	58–4155 (17)	23–1489 (70)	58–8071 (23)
Total Nitrogen (mg/L)	2.7–148.0 (14)	2.5–10.4 (5)	0.5–65.0 (5)	2.8–31.0 (11)	1.3-148.0 (28)	0.5-65.0 (16)
Total Phosphorus (mg/L)	0.1-60.0 (17)	0.3-2.6 (5)	2.7-187.0 (5)	0.2-51.6 (13)	0.1-60.0 (27)	0.2-187.0 (18)

Another study was conducted by (Friedler, 2004) to characterize the quality and quantity of individual domestic greywater streams. The kitchen sink, washing machine, and dishwasher were found to be major contributors of pollutants, while the wash basin was the least polluting appliance. Greywater can make up 55-70% of the specific daily load of TSS and BOD in municipal sewage. To reduce pollutants in greywater, 18 scenarios were studied in which at least one stream was excluded from the combined greywater stream. Excluding the kitchen

sink, washing machine, and dishwasher significantly improved greywater quality while still providing enough greywater for reuse.

3.3.2. Greywater Reuse and Treatment Technologies

Recycled wastewater finds primary reuse in two main applications: toilet flushing and irrigation. However, instant recycling of greywater may pose risks to both human health and the environment (Maimon et al., 2010). Risks to human health is due to pathogens present in greywater can lead to illnesses either through direct exposure or by consuming plants contaminated with these pathogens (Shuval et al., 1997) and the environment may face potential risks from high levels of surfactants, oils, boron, and salts, which have the potential to change soil properties, harm plant life, and contaminate groundwater. Therefore, treatment of greywater before reuse is essential to reduce the hazards (Gross et al., 2005).

Greywater treatment technologies can be either physicochemical or biological. Physicochemical techniques utilize physical and/or chemical processes such as filtration, adsorption, and reverse osmosis. While biological methods for treating greywater use a mix of microorganisms, sunlight, and controlling oxygen levels. Some examples of these systems include activated sludge systems, trickling filters, waste stabilization ponds, rotating biological contactors, and various others (Oteng-Peprah et al., 2018).

Constructed wetlands have been studied to be an effective technology for treating greywater using a combination of physical, chemical and biological processes to remove pollutants, and especially effective in removing BOD_5 (Oteng-Peprah et al., 2018). Other methods of greywater treatment include the application of advanced oxidation processes like ozonation, granular activated carbon, and ultrafiltration for greywater treatment, demonstrating the efficacy of chemical-based technologies in improving water quality (Shahsavani et al., 2022).

3.4. Modelling water flow and nutrient transport in variably saturated porous media

As green roof technology progresses, the need for predicting its performance increases, and computer models can be an effective tool to simulate water balances and evaluating the effect of each influencing factor of the green roof. According to a review paper by (Li & Babcock, 2014) the most commonly used computer models to simulate green roofs are EPA's Stormwater management model (SWMM), Soil water atmosphere and plant (SWAP), Soil-

Water Movement Simulator in Two Dimensions (SWMS2D), and HYDRUS. Comparison of each of the software is shown in table 3.

Table 3 A summary of commonly used numerical models, Adapted from (Li & Babcock, 2014)

	SWMM	**SWAP (Swatre)**	**SWMS-2D**	**Hydrus**
Developer	USEPA	Wageningen Agricultural University	USDA-ARS US Salinity Laboratory	USDA/USSL Riverside, California
Accessibility	Free to download	Free to download	Free to download	Free for 1D only
Dimension	1D	1D, 2D	2D	1D, 2D, 3D
Main application	Dynamic precipitation-runoff simulation	Transport of water, solutes and heat in unsaturated/saturated soils	Transport of water, solutes and heat in unsaturated/saturated soils	Transport of water, solutes and heat in unsaturated/saturated soils
Scale	Site and regional	Site	Site	Site
Input requirements	Precipitation and site properties	Spatial, temporal, soil, solute, and plant properties	Spatial, temporal, soil, solute, and plant properties	Spatial, temporal, soil, solute, and plant properties
Main simulation processes	Collection of schematic sub-catchment areas that receive precipitation and generate runoff and pollutant loads	Saturated-unsaturated water flow, soil heat flux, convection, diffusion and dispersion, linear, non-linear adsorption, first-order decomposition and root uptake of solutes	Saturated-unsaturated water flow, soil heat flux, convection, diffusion and dispersion, linear, non-linear adsorption, first-order decomposition and root uptake of solutes	Saturated-unsaturated water flow, soil heat flux, convection, diffusion and dispersion, linear, non-linear adsorption, first-order decomposition and root uptake of solutes

Storm Water Management Model SWMM:

The Storm Water Management Model (SWMM) is a widely recognized and utilized tool for urban drainage design and planning (Niazi et al., 2017). The model has been employed to simulate the hydrological performance of green roofs, including extensive green roofs, by integrating the Low Impact Development (LID) Controls module that allows for the consideration of various types of technological solutions known as LID practices, such as infiltration trenches, vegetative swales, and bio-retention cells, in the catchment model. These LID practices provide storage, infiltration, and evaporation of both direct rainfall and runoff captured from surrounding areas. The general structure of LID controls in SWMM consists of four layers: surface layer, soil (substrate) layer, storage layer, and under-drains (Burszta-Adamiak & Mrowiec, 2013).

(Cipolla et al., 2016) conducted a study to evaluate hydrological performance of a full-scale extensive green roof in Bologna, Italy and used commercial software of Storm Water Management Model (SWMM) to assess the suitability of the model to simulate the long-term hydrologic response of green roofs.

For the duration of one year, starting from January and ending in December 2014, continuous weather data and runoff were gathered, leading to 69 storm events that were applicable for analysis. The experimental data show that the attenuation of individual event rainfall fluctuated from 6.4% to 100%, with an average annual value of 51.9%. Furthermore, the research utilized the field data to calibrate and verify a numerical model, which was developed using the commercial software SWMM 5.1. This model was employed to simulate the long-term hydrologic response, covering a period of one year, for the same full-scale extensive green roof and to compare it with an adjacent impervious roof of the same size.

Results demonstrated that the proposed model has good capabilities in generating the stormwater runoff hydrograph for green roofs throughout the year. This was evident through the high NSE values and low RSR values during both the calibration and validation stages. Moreover, the small difference (less than 9%) in total retention between the 69 measured and simulated events verified the model's reliability for long-term predictions. The presented modeling approach indicates that SWMM can be employed to evaluate the effectiveness of LID systems (Low Impact Development) The results of the study are illustrated in Figure 5, where the rainfall patterns and corresponding measured runoff (shown by the grey area) are compared with the simulated runoff (represented by the black line) for the Sedum green roof during four calibration events. These events took place on: a) February 10th, 2014; b) November 17th, 2014; c) June 14th, 2014; and d) September 20th, 2014.

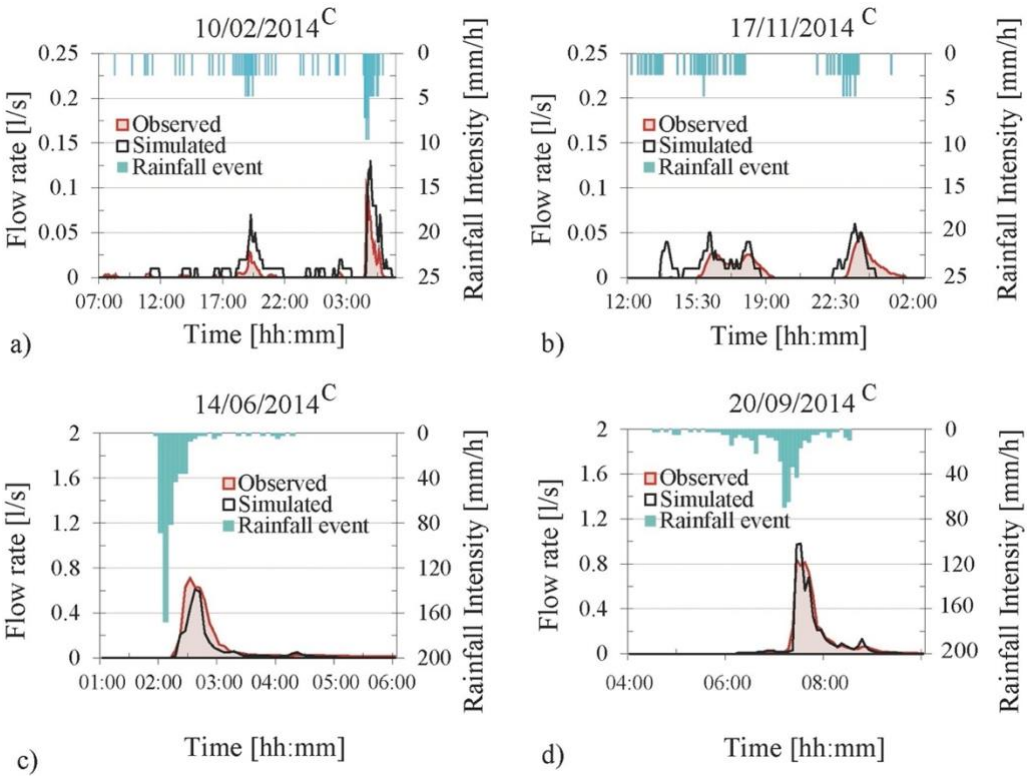

Figure 5 The rainfall patterns and the corresponding measured runoff, adapted from (Cipolla et al., 2016)

Soil water atmosphere and plant (SWAP):

SWAP is a model that simulates the movement of water, solutes, and heat in both unsaturated and saturated soils with high precision (Li & Babcock, 2014). The upper boundary conditions in the model are determined by meteorological variables, including radiation, humidity, wind speed, temperature, and precipitation, which are used to calculate evapotranspiration through the Penman–Monteith equation. The lower boundary conditions can be a groundwater table at infinity, a seepage face, or a fixed pressure head or upward flux, which can lead to oversimplification in some cases. The required soil properties are hydraulic conductivity and water retention curve. The outputs include suction, substrate water storage, evapotranspiration, and drainage profiles. SWAP also provides detailed soil moisture information, which can aid in selecting appropriate plants (Li & Babcock, 2014).

Soil-Water Movement Simulator in Two Dimensions (SWMS2D):

SWMS-2D is a highly accurate tool that can accurately simulate many factors affecting green roof systems. It models saturated and unsaturated water flow in two-dimensional porous media at a site-specific scale (Li & Babcock, 2014).The program offers a variety of upper and lower boundary conditions, including constant head, constant flux, atmospheric boundary, variable

head, or variable flux. The required input data include climate conditions such as precipitation and evapotranspiration, as well as soil hydraulic conductivity and water retention parameters. The output data include various hydrologic properties, such as discharge hydrograph, discharge volume, peak flow rate, and hydrograph centroid (Li & Babcock, 2014).

SWM II

(Vogel, 1987) developed a numerical model or simulating two-dimensional flow in variably saturated porous media utilizing Richards' equations to describe water flow within the dual-permeability medium. A study by (Vogel et al., 2000) modified the SWM II finite element code to handle a 2D dual-permeability model incorporating both water and solute transfer between fracture and matrix domains. The study compares single- and dual-permeability approaches for modeling variably saturated flow and transport in two-dimensional heterogeneous soil systems by simulating five different scenarios. Results showed that dual-permeability models significantly enhance the simulation of water and solute movement, with faster and larger leaching compared to single-permeability models. Preferential pathways for water and solute transport were more pronounced in scenarios with spatial variability in hydraulic conductivity, emphasizing the importance of considering both spatial variability and soil structure.

3.5. HYDRUS

The HYDRUS numerical models are extensively utilized for the simulation of water flow and solute transport in soils and subsurface that have varying levels of saturation (Langergraber & Šimůnek, 2012) These models are applied to a diverse array of water flow, solute transport, and heat transfer problems, which can be either steady-state or transient in nature. They are used for both simple, one-dimensional laboratory column flow or transport simulations over a short period of time, as well as more intricate, long-term, multi-dimensional field studies (Langergraber & Šimůnek, 2012). HYDRUS numerically solves the Richards' equation for saturated–unsaturated water flow and uses convection–dispersion equations for heat and solute transport (Šimůnek et al., 2016).

Different HYDRUS packages serve different purposes and are all widely used in modelling of green roofs. The HYDRUS-1D software package can be used to simulate water flow, solute transport, heat transport carbon dioxide transport in variably saturated media while assuming either a vertical, horizontal, or generally inclined direction. HYDRUS (2D/3D) on the other

hand is capable of modeling water flow and solute or heat transfer in two-dimensional vertical or horizontal planes, in axially symmetric three-dimensional spaces, or in fully three-dimensional variably saturated domains (Li & Babcock, 2014).

3.5.1. Case Studies of Green roof modelling with HYDRUS:

(Hilten et al., 2008) conducted a study in Athens, Georgia, USA to evaluate the effectiveness of green roofs in mitigating stormwater and used HYDRUS-1D to simulate runoff and actual evapotranspiration for the study site during June 2005.

The study site consisted of one hundred square green room blocks of dimensions 60 × 60 × 10 cm with a total green roof area of 37 m^2. Green roof blocks were filled with engineered soil of 80% expanded slate and 20% organic matter. Results of the simulated HYDRUS model were then verified with on-site measured runoff data. The study found that the depth of rainfall per storm has a significant impact on the effectiveness of green roofs in managing stormwater. Specifically, green roofs can completely retain small storms that measure less than 2.54 cm in depth, while they can detain larger storms. These findings are based on the assumption that the average moisture content is approximately 10% before the storm. Figure 6 illustrates hydrographs generated by HYDRUS results and SCS-synthesized storms, displaying cumulative runoff (solid line), cumulative rainfall (x-symbols), instantaneous runoff (thick dashed line), and instantaneous rainfall (thin dashed line) across different rainfall intensities: (a) 2.54 cm, (b) 3.81 cm, (c) 5.08 cm, and (d) 7.93 cm.

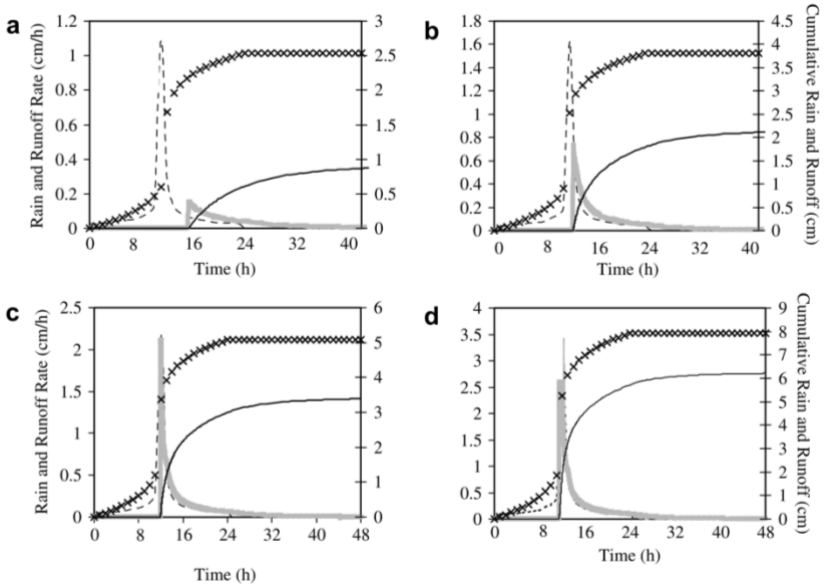

Figure 6 Modeled hydrographs displaying cumulative runoff, Adapted from(Hilten et al., 2008)

A study by (Gärdenäs et al., 2005) tested fertigation, the technique of supplying dissolved fertilizer to crops through an irrigation system, aiming to assess the effects of fertigation and soil type on nitrate leaching potential. Nutrients were placed near plant roots in a controlled manner to reduce fertilizer losses that normally occur through leaching into the groundwater. HYDRUS-2D was used and was able to accurately simulate solutes transport in the root zone. To evaluate water and nutrient use efficiency and nitrate leaching, four of the most typically used pressurized irrigation systems in California, USA were presented: surface drip tape, subsurface drip tape, surface drip emitter, and micro-sprinkler. Irrigation with fertigation was simulated for a period of 28 days after 56 days of flow-only simulations, to approach a 'pseudo-equilibrium' condition. Results show that seasonal leaching of nitrates was highest in coarse-textured soils and surface water ponding enhanced water spreading across the surface, leading to downward infiltration and horizontal spreading of soil nitrate while surface-applied irrigation systems on finer-textured soils increased lateral spreading of water and nitrates. Fertigation at the beginning of irrigation cycles tended to increase seasonal nitrate leaching while fertigation at the end of irrigation cycles reduced potential nitrate leaching. Figure 5 shows the water balance findings for each of the four micro-irrigation systems and soil types, as a percentage of the total water applied over the 28-day period.

Another study by (Brunetti et al., 2021) investigates the potential of using green roofs for domestic wastewater treatment and nitrogen removal, aiming to explore the hydrological, energetic, and water quality benefits. By integrating both experimental and numerical approaches to better understand reactive transport processes in green roofs. The experimental setup consisted of 15 cm-deep green roof testbeds with and without vegetation and were then injected with domestic wastewater. Inorganic nitrogen compounds (ammonium, nitrite, nitrate) were monitored weekly in the outflow and analyzed using UV-VIS spectrophotometry. Using HYDRUS-1D, a mechanistic numerical model is then calibrated against multiple observations from the experiment. Results showed that nitrification capacity of green roofs increases after wastewater application. In a non-vegetated green roof, 94% of the total injected nitrogen leaches out, whereas in a vegetated GR, the leaching rate is 67%. There is a negative correlation between nitrate leaching and the vegetation's ability to take up solutes, which can account for up to 32% of the total injected nitrogen. Enhancing this uptake capacity is beneficial and can be accomplished by carefully choosing plant species and minimizing water stress through proper irrigation scheduling.

3.5.2. HYDRUS Wetland Module

The HYDRUS Wetland Module is a specialized tool developed to simulate the biological and chemical processes involved in treating wastewater in subsurface flow treatment wetlands (SSF TW) (Pucher & Langergraber, 2018). The HYDRUS Wetland Module offers a comprehensive simulation of aerobic, anoxic, and anaerobic transformation and degradation processes for organic matter, nitrogen, phosphorus, and sulfur during the treatment of polluted wastewater in subsurface constructed wetlands (Šimůnek et al., 2016). It includes two biokinetic models designed to describe the transformation and degradation processes in constructed wetlands treating wastewater which are CW2D and CWM1, for the simulation of reactive transport in Constructed Wetlands. CW2D takes into account aerobic and anoxic transformation and degradation processes of organic matter, nitrogen, and phosphorus, while CWM1 includes aerobic, anoxic, and anaerobic processes for organic matter, and sulfur (Langergraber & Šimůnek, 2012).

A study by (Langergraber & Šimůnek, 2012) utilized these models to simulate horizontal flow constructed wetlands, with the HYDRUS system capable of modeling fixed biomass, which is essential for reliable predictions of treatment efficiency. Simulation results indicated that CWM1 provided more realistic outcomes, as it accounts for anaerobic degradation processes. The researchers also investigated the influence of wetland plants and found considering plant effects to be important since the release of O_2 from wetland plant roots influences the simulation results.

4. THEORY OF WATER FLOW AND NUTRIENT TRANSPORT IN UNSATURATED ZONE

The Unsaturated zone, also called vadose zone or partially saturated zone of the earth's crust is the region bound by the soil surface at the top and water table at its bottom. Saturation degree of the unsaturated zone is highly influenced by hydrological processes such as precipitation, infiltration, evaporation, and plant water uptake. The unsaturated zone serves as a critical interface between the land surface and groundwater, influencing water movement, nutrient transport, and ecosystem functions. Understanding the presence and flow of water in this zone is crucial for managing water resources and predicting hydrological changes. Therefore, this chapter studies the processes happening in the unsaturated zone as well as numerical approaches for modelling.

4.1. Water Flow in Unsaturated Zone

4.1.1. Forces acting on water particles in soil

The gaps or empty spaces amongst the particles of soils and other grainy substances are known as pores. A significant characteristic of water-holding structures is their porosity. A soil's porosity is mainly influenced by its particle size distribution and structure and can be computed using the formula (Brutsaert, 2005):

$$n = \frac{Vp}{V} \qquad (1)$$

Where n denotes porosity of the soil, is Vp the volume of the pores, and V is the total volume of the porous media.

Pores in the soil have the ability to retain water which can be used by plants, and the retention of water particles is influenced by the forces acting on them. These forces are gravitational forces and retention forces. Retention forces can be further divided into capillary and adsorptive forces and act against gravitational forces to bind water in the soil.

Capillary forces are the attractive forces between water molecules and solid particles of the soil. These forces arise due to the surface tension of water and the interactions between water molecules and the solid material. Capillary forces play a crucial role in determining the movement and distribution of water in soil pores.

Water contained within the pores between soil particles, forms a meniscus at the edges where the liquid meets the solid surface. The curvature of this meniscus generates a pressure difference across the interface due to surface tension (Hillel, 2003), as shown in Figure 7. This phenomenon is described by the Young-Laplace formula:

$$\Delta P = \frac{2\gamma \cos \alpha}{r} \qquad (2)$$

Where ΔP represents the pressure difference across the interface which is also referred to as capillary pressure and is directly proportional with γ , surface tension and inversely proportional with r, radius of the capillary.

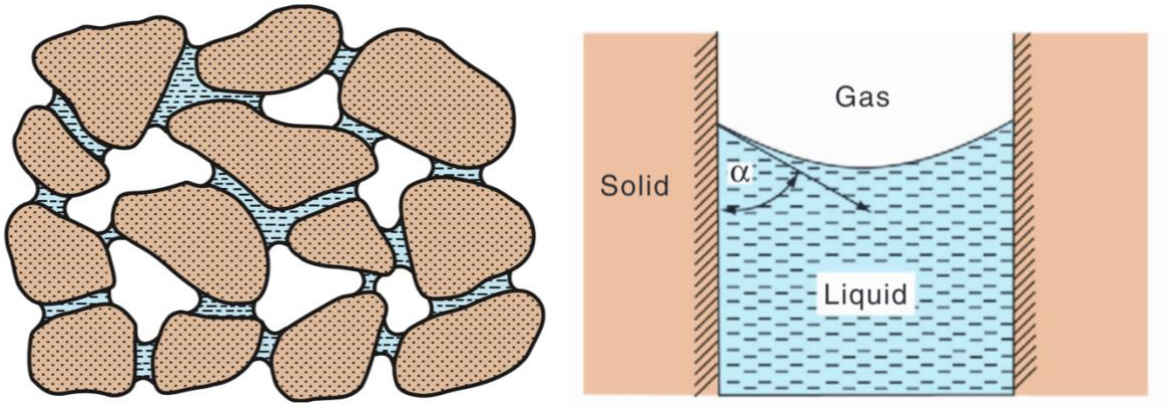

Figure 7 Water contained in the porous media Adapted from (Hillel, 2003)

4.1.2. Soil Water State Variables:

Total Water Potential

Total water potential in porous media generally denoted by ϕ refers to the sum of all factors influencing the movement of water within the medium and is described by (Eq. 3) below. It is a combination of gravitational potential, pressure potential, osmotic potential, and matric potential.

$$\phi_t = \phi_g + \phi_P + \phi_O + \cdots \qquad (3)$$

- Gravitational potential accounts for the effect of gravity on water movement. This potential is calculated for each location in soil water based on its height above a chosen reference point.
- Pressure potential represents the pressure exerted by water within the pores which can also be matric potential considering the capillary forces exerted by the medium's structure on water. This potential reflects the energy required for water retention in the soil. The pressure potential in soil water varies depending on the hydrostatic pressure relative to atmospheric pressure. When soil water experiences hydrostatic pressure greater than atmospheric, the pressure potential is positive; and when it experiences pressure lower than atmospheric, known as tension or suction, the pressure potential is

negative. Matric potential arises from capillary and adsorptive forces between water and the soil matrix, resulting in negative gauge pressure. Water pressure potential varies with height relative to the free-water surface, as shown in Figure 8, with zero potential at the surface, positive potential below, and negative potential above (Hillel, 2003).

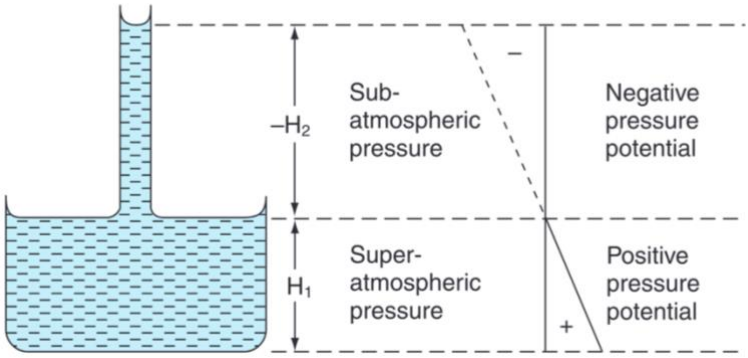

Figure 8 Atmospheric pressures below and above a free water level, Adapted from (Hillel, 2003)

- The osmotic potential is determined by the difference in solute concentrations across a membrane, which selectively allows water to pass through more easily than salts, resulting in an imbalance that drives water movement.

Soil Moisture Content (θ): refers to the portion of soil voids filled with water rather than air. When the soil is saturated, the moisture content is equivalent to the porosity of the soil, and is described by (Chow et al., 1988) with the following equation:

$$\theta = \frac{Volume\ of\ Water}{Total\ Volume} \qquad (4)$$

4.1.3. Soil Hydraulic properties:

Hydraulic Conductivity K: is the ability of the porous medium to conduct liquids. It is defined as the volume of water that can flow through a unit cross-sectional area of the medium in a unit time under a unit hydraulic gradient. Hydraulic conductivity is influenced by various factors, including the porosity, grain size distribution, and connectivity of the pore spaces within the medium. Soil hydraulic conductivity is typically measured in laboratory and field tests, quantified in terms of length units per unit of time (m/s).

Hydraulic conductivity can be described in terms of pressure head K(h) in variably saturated soils, as it describes how the conductivity of the medium changes with alterations in the pressure head of the fluid within it. Saturated hydraulic conductivity K_{sat} on the other hand, represents saturated hydraulic conductivity, denoting the maximum rate at which water can flow through a fully saturated porous medium under the influence of gravity alone.

Retention Curve: is relationship between soil moisture content or degree of saturation and suction in equilibrium. The retention curve illustrates how water is held within the pore spaces of a porous medium against the force of gravity. As water is added to or removed from the soil during wetting and drying processes, the pressure or suction exerted on the water influences its retention characteristics (Braddock et al., 2001). This relationship is shown in Figure 9.

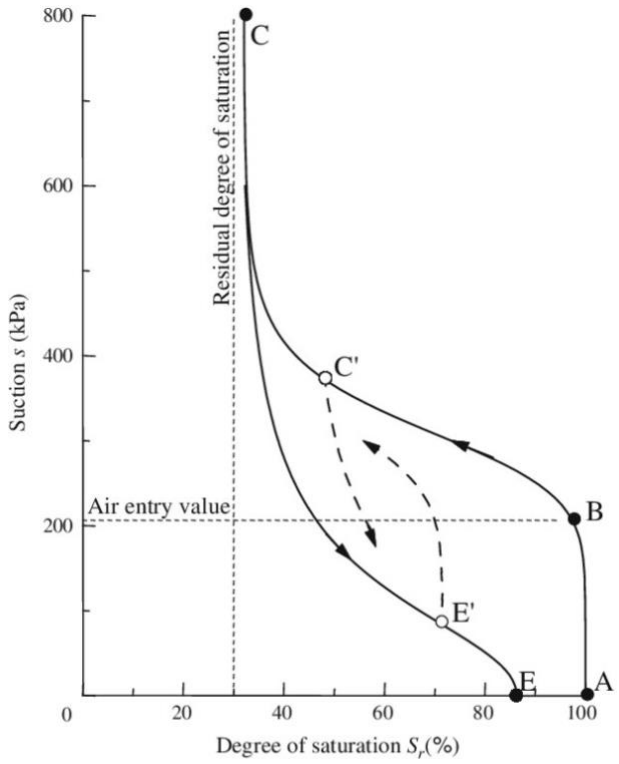

Figure 9 A typical soil water retention curve. Adapted from (Masrouri et al., 2008)

Various mathematical expressions are commonly employed to describe the soil water retention curve and parameterize them. These expressions allow measured data points to be fitted, aligning them with the mathematical representation. Expressions such as the Brooks and Corey

formula has the ability to predict the hydraulic properties of soil by interpolating points along the retention curve. The equation is formulated as follows (Brooks & Corey, 1964):

$$\theta_e(h) = \begin{cases} \left(\frac{H_b}{h}\right)^{\lambda} & h < H_b \\ 1 & h \geq H_b \end{cases} \quad (5)$$

Where λ, H_b are parameters of the model standing for pore size distribution index and bubbling pressure, respectively. $\theta_e(h)$ represents effective moisture content in terms of pressure head and the effective moisture content in terms of volumetric water content can be expressed as:

$$\theta_e = \frac{\theta - \theta_r}{\theta_s - \theta_r} \quad (6)$$

Where θ_s is the saturated moisture content and $\theta_r$is the residual moisture content.

Another widely used expression to fit measured data is the (van Genuchten, 1980) which provides a flexible and accurate way to describe the retention curve by considering a non-linear relationship between soil moisture and pressure head:

$$\theta_e = \left[\frac{1}{1 + (\alpha h)^n}\right]^m \quad (7)$$

Where α, n, and m are parameters of the model, h is the pressure head, and θ_s and θ_r are the saturated and residual moisture content.

4.1.4. Water Flow Equations

Darcy's Law: explains flow of water through porous media and was formulated based on experiments on the seepage of water through a sand-filled pipe in 1856, which can be represented by the following equation (Brutsaert, 2005):

$$Q = \frac{KA(H1 - H2)}{\Delta L} \quad (8)$$

The relationship shows that the flow rate Q of water through a porous medium (such as sand) is directly proportional to the cross-sectional area A and the difference in hydraulic head H, and inversely proportional to the length L of the medium.
Specific Discharge Rate (Q /A), also known as flux density q or simply flux, measures the flow intensity at a specific point or within a specific volume of porous media. Flux q is the flow rate per unit area, indicating how much water passes through a given area in a given time. Darcy's law leads to the expression:

$$\mathrm{q} = K_{sat}\,\Delta\mathrm{H}/\mathrm{L} \qquad (9)$$

Where q represents flux, K_{sat} is saturated hydraulic conductivity, ΔH is the change in hydraulic head, and L is the length of the medium.

The Darcy-Buckingham law for water movement in unsaturated soil is a generalized version of Darcy's law that applies to unsaturated flow. It was introduced by Edgar Buckingham in 1907 and is sometimes called the Darcy-Buckingham equation. The law states that the flux of water in unsaturated soil is proportional to the gradient of a potential, which is a function of the water content and pressure head. The law takes into account the fact that the hydraulic conductivity of unsaturated soil depends on the water content, and it allows for the prediction of water flow in unsaturated soil as a function of time and space (Nimmo & Landa, 2005).

$$\mathrm{q} = \mathrm{K}(\theta)\,\Delta\mathrm{H}/\mathrm{L} \qquad (10)$$

Where q is the volumetric flux density of water, K is the hydraulic conductivity as a function of θ, the volumetric soil water content. ΔH is the change in hydraulic head, and L is length of the medium.

Continuity Equation: The general mass balance equation of a phase, the rate of change of water storage in a given volume of soil or aquifer is equal to the sum of the inflow and outflow rates of water, accounting for any sources or sinks of water within that volume. In its simplest form the continuity equation is formulated as:

$$\frac{\partial\theta}{\partial t} = -\frac{\partial q}{\partial z} \qquad (11)$$

Where θ represents the volumetric soil water content, t stands for time, q is the volumetric flux density of water and z the vertical coordinate.

Richard's Equation: The equation describing the flow of water within a porous medium which is a partial differential equation that combines Darcy's law with the continuity equation. Richards equation accounts for changes in state variables such as water content, pressure, and velocity over time and space within a given flow domain neglecting the flow of non-wetting space, which is usually air by disregarding the pressure difference needed to make the gas phase flow because of the large difference in water and gas mobility (Farthing & Ogden, 2017). The equation's one-dimentional form is formulated as:

$$\frac{\partial \theta}{\partial_t} = \frac{\partial}{\partial_z}\left(K\frac{\partial h}{\partial z} + K\right) \qquad (12)$$

Where θ represents the volumetric soil water content, t stands for time, z the vertical coordinate, h the pressure head, and K is the hydraulic conductivity.

4.1.5. Processes in the porous media

Evapotranspiration

Evaporation is the process through which liquid water at the soil surface transitions into vapor and enters the atmosphere. When the surface of the soil is covered with vegetation, a process called transpiration, which is evaporation from plants, is the main mechanism of soil-water leaving to the atmosphere (Hillel, 2003). The two processes combined results in evapotranspiration.

The Penman-Monteith equation is a widely used empirical equation for estimating evapotranspiration rates. It is based on the principle of energy balance and considers various climatic factors and surface characteristics that influence evapotranspiration. The Penman-Monteith equation is expressed as follows (Zotarelli et al., 2010):

$$ET_0 = \frac{0.408\Delta\,(R_n - G) + \gamma \frac{900}{T + 273} u_2\,(e_s - e_a)}{\Delta + \gamma(1 + 0.34\,u_2)} \quad (13)$$

ET_0 represents reference evapotranspiration which is the rate at which easily accessible soil moisture evaporates from designated vegetated areas. Δ is the slope of the vapor pressure curve, R_n is net radiation at the crop surface, and G represents soil heat flux density. T stands for mean daily air temperature at 2 m height, u_2 for wind speed at 2 m height, e_s for saturation vapor pressure, and e_a represents actual vapor pressure.

γ denotes the psychrometric constant which relates the water vapor pressure in the air to air temperature, allowing estimation through temperature readings from dry and wet thermometers; it is commonly approximated to be 0.000665 P, P representing atmospheric pressure (Zotarelli et al., 2010)

Infiltration

Infiltration describes the movement of water from the ground surface into the soil, a process influenced by various factors such as soil condition, vegetative cover, soil properties like porosity and hydraulic conductivity, and the current soil moisture content. This complex process can be approximately explained with mathematical description. The distribution of soil moisture during water infiltration is characterized into four zones within the soil profile as shown in Figure 10: a saturated zone near the surface, a transmission zone with uniform moisture content, a wetting zone where moisture diminishes with depth, and a wetting front characterized by a sharp moisture content transition (Chow et al., 1988).

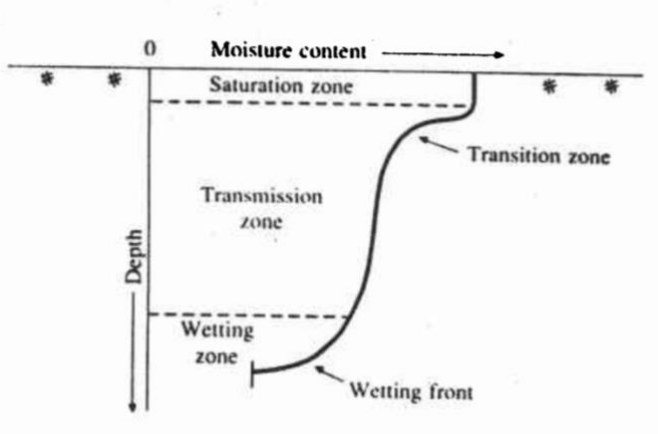

Figure 10 Soil moisture distribution during infiltration, adapted from (Chow et al., 1988)

Horton's Equation, developed by (Horton, 1933) describes the earliest infiltration model, observing that infiltration initiates at a certain rate i_0 and decreases exponentially until stabilizing at a constant rate i_c (Chow et al., 1988):

$$i(t) = i_c + (i_0 - i_c)e^{-kt} \quad (14)$$

$$I(t) = i_c\, t + \frac{i_0 - i_c}{k}\,(1 - e^{-kt}) \quad (15)$$

The infiltration rate $i(t)$ measured in centimeters per hour, represents the speed of water ingress at the soil surface, while the cumulative infiltration $I(t)$ accumulates the depth of water infiltrated over a specified period, calculated as the integral of the infiltration rate. i_0 is the initial intensity and i_c is the steady state intensity. k represents the decay constant.
Other models commonly used to describe infiltration are Philip, Green-Ampt, and Richard's Equation models.

4.2. Solutes Transport in Unsaturated Zone

Solute transport in the unsaturated zone is governed by complex interactions between soil properties, hydraulic processes, and chemical characteristics of the solutes. The movement of solutes in this zone is influenced by advection, dispersion, diffusion, and chemical reactions, all of which contribute to the overall transport behavior (Bear & Cheng, 2010).

Advective fluxes: the movement of solutes with the bulk flow of water through the soil matrix. In the unsaturated zone, this process occurs primarily due to variations in soil water content and gradients in matric potential and the flux density of solute advection follows the principle of darcy's law.

$$j_{A = cq} \quad (16)$$

j_A represents advective flux, c is concentration of the solute and q is flux density.

Hydrodynamic dispersion which the spreading out or mixing of solutes within the flowing fluid as it moves through the porous medium can be described either in or molecular diffusion or mechanical dispersion:

Diffusive Flux: Diffusive flux refers to the movement of solute particles from regions of higher concentration to regions of lower concentration, driven by the concentration gradient. This process is governed by Fick's law of diffusion where the diffusive flux is proportional to the negative gradient of the concentration (Bear & Cheng, 2010):

$$j_d = -\theta \boldsymbol{D_d} \frac{\partial c}{\partial x} \qquad (17)$$

j_d represents diffusive flux, θ is the volumetric fraction of the considered phase, and c is concentration of the solute. $\boldsymbol{D_d}$ is the tensor of molecular diffusion and can be obtained by considering the effect of tortuosity.

Dispersive Flux: Mechanical dispersion is distinguished from diffusion by considering it as the spreading of solute due to velocity variations at different points in the porous medium. It includes both mechanical dispersion and molecular diffusion (Sposito et al., 1979).

$$j_m = -\theta \boldsymbol{D_m} \frac{\partial c}{\partial x} \qquad (18)$$

j_m represents mechanical dispersive flux, θ is the volumetric fraction of the considered phase, and c is concentration of the solute.

$\boldsymbol{D_m}$ is the tensor of molecular diffusion, and considers Longitudinal and Transversal Dispersivity, explained by (Bear & Verruijt, 1987) in the following equations:

$$D_L = \alpha_L \, v \,, \quad D_T = \alpha_T \, v \qquad (19)$$

Where D_L and D_T are coefficients of longitudinal and transverse dispersivity, α_L and α_T represent dispersivity in the direction of mean flow, and perpendicular to the direction of mean flow, respectively, and v is the mean pore velocity. Gelhar et al. (1992) proposed a general relationship where longitudinal dispersivity is approximately 10% of the length scale, and is 10-15 times larger than the transverse dispersivity.

Advection-Dispersion-Equation (ADE): is a partial differential equation that combines the principles of mass conservation with the effects of advection and dispersion to describe the transport of solutes in the porous medium.

$$\frac{\partial(\theta c)}{\partial t} + div(cq) - div(\theta D\ grad\ c) = 0 \qquad (20)$$

Where θc represents the mass of solute per unit volume of the porous medium, $div(cq)$ the divergence of the advective flux, and $div(\theta D\ grad\ c)$ the divergence of dispersive flux.
θ is the porosity of the medium, c is the solute concentration, q is water flux density, D is the coefficient of dispersion.

Sorption: The process of exchange of solutes between the liquid phase and the solid phase in variably saturated zone. This process can include adsorption, where solutes adhere to the surface of solid particles, absorption, where solutes penetrate into the solid matrix, and desorption, where solute particles attached to solid particles are released into the water phase. The quantity of solute that the solid phase adsorbs typically depends on the solute's concentration in the solution. This relationship is described by an adsorption isotherm which is determined experimentally (Císlerová & Vogel, 1998).

Degradation: The theory of movement and transformation of contaminants as they travel through a porous media. The first-order degradation rate law is widely used to describe the degradation of various contaminants, including pesticides, nutrient chemicals like nitrate, and contaminants such as PAHs.
The rate of decay in a first-order process is directly proportional to the concentration of the solute. The general form of the first-order decay equation is (Gajewska et al., 2020)

$$A_h = Q_d * (\ln c_{in} - \ln c_{out})/k \qquad (21)$$

where A_h is the surface area, Q_d is the average flow rate. c_{in} is the influent solute concentration, c_{out} is the effluent solute concentration, and k is the first-order rate constant, representing the degradation rate.

5. METHODOLOGY

This chapter presents the methodology employed in this study to construct a HYDRUS-2D model based on an experiment conducted by Petreje et al. (2023). It covers experimental setup of the hybrid green roof, model development, and set up for simulations of water flow and solute transport. The study 'Performance study of an innovative concept of hybrid constructed wetland-extensive green roof with growing media amended with recycled materials' explores a hybrid green roof system that integrates recycled materials into growing media and employs greywater for irrigation. This experiment was chosen to be modeled with HYDRUS to extend the hybrid green roof concept towards practical application and create a digital twin, providing a comprehensive evaluation of the system's hydraulic and hydrological performance. The study found that growing media which contained recycled materials in this study exhibit hydro physical properties comparable to commercially available ones, and that the constructed wetland effectively reduces nitrogen and orthophosphate concentrations in pre-treated greywater. Given the complexity of the system and the need for accurate modeling, HYDRUS is chosen as the modeling platform due to its reliable capabilities in simulating water flow and nutrient transport in constructed wetlands and green roofs.

5.1. Experimental Setup

The study was performed by team of Czech Technical University in Prague (UCEEB and Faculty of Civil Engineering) in cooperation with Brno University of Technology (VUT), Brno, Czech Republic with the location on the premises of VUT having direct exposure to sunlight from June to October, 2020. The estimated annual solar radiation is 995 W/m2/year. Recorded data from the Brno-Turany station, located approximately 12 km away, during the period between 1981 and 2010, indicated an average annual air temperature of 9.4 ◦C and precipitation of 500 mm. The experimental arrangement featured two outdoor hybrid green roof test beds, each consisting of two parts, a constructed wetland, and an extensive green roof. Pre-treated greywater stored in a storage tank was channeled into the contracted wetlands, where the greywater was further treated and then distributed evenly over the extensive green roofs through 16 v-notch weir gates. Figure 11 shows a photograph of the setup of the hybrid green roof test beds.

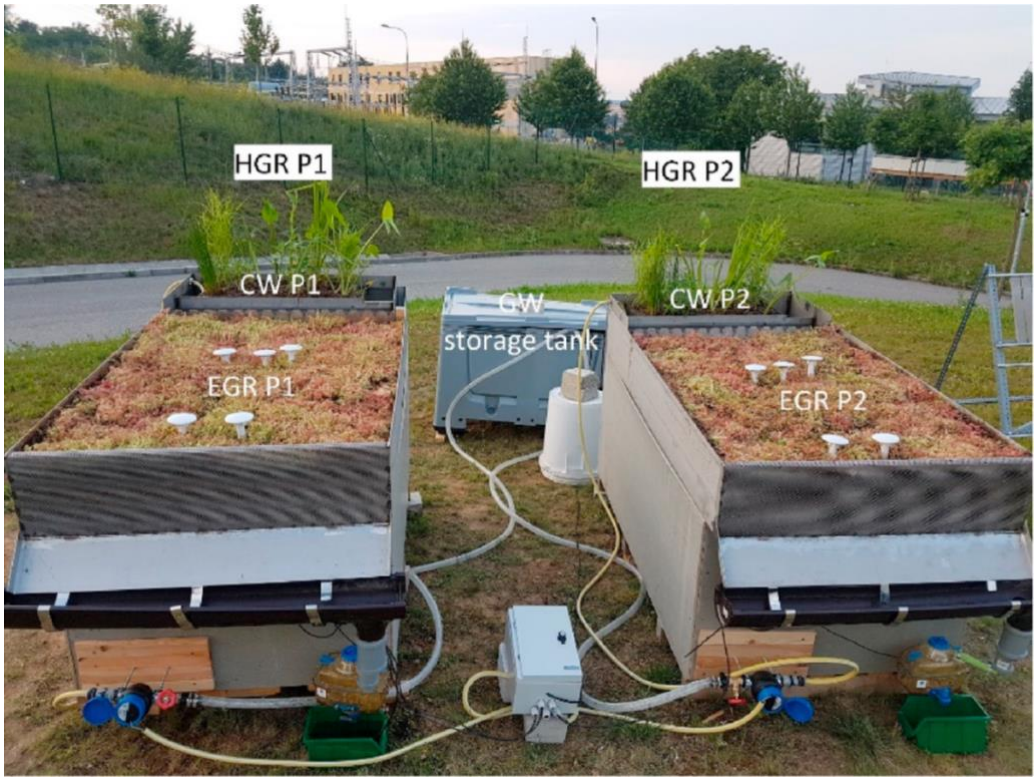

Figure 11 Photograph of the two hybrid green roof testbeds, adapted from (Petreje et al.,2023)

The first part of each test bed measuring (450 × 994 mm^2) consisted of three flumes and a water distribution channel with a depth of 300 and a water level of 250 mm. The first flume was filled with water and distributed the water into the second flume which was the constructed wetland filled with expanded clay balls with macroporosity 49% and vegetation. From there, water flowed into the third chamber and eventually into the distribution channel to irrigate the extensive green roof section measuring (1397 × 994 mm^2) positioned at a slope of 5%. The extensive green roof consisted of four layers: a 3 mm thick geotextile at the bottom, followed by 50 mm of mineral wool, then 100 mm of growing media containing recycled materials, topped with a 25–40 mm vegetation mat. These measurements are demonstrated in Figure 12.

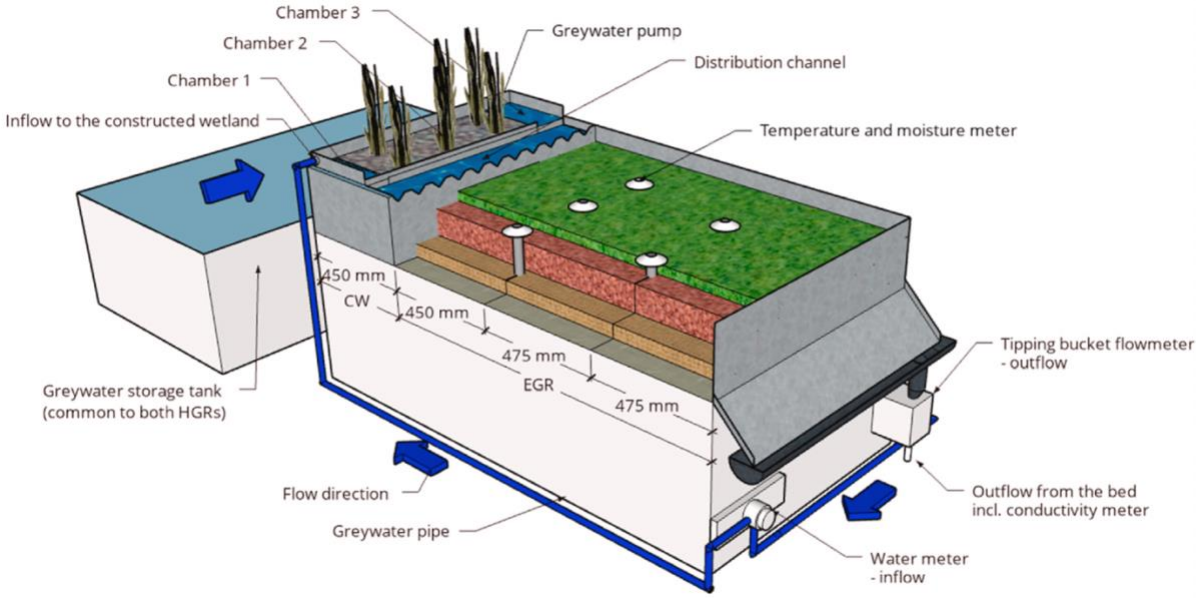

Figure 12 Diagram of the test bed of the hybrid green roof, adapted from (Petreje et al.,2023)

Irrigation was conducted using greywater at a rate of 10L/day applied in a single dose during one minute to supply water to the experimental extensive green roofs as part of the research experiment while measuring the inflow and outflow rates using water meters. Temperature and water content were measured using sensors placed at various depths within the green roofs. These sensors were modified for horizontal installation and positioned at specific points to capture data from different layers of the green roofs. Additionally, temperature data were collected to evaluate the thermal regime of the green roofs, with selected daily intervals fitted with a sine function model for analysis. An electrical conductivity probe was also utilized to measure the electrical conductivity of the outflowing water from one of the green roofs.

5.2. Model Development

HYDRUS-2D was chosen for numerical modelling of the semi intensive part of hybrid green roof due to the capability of two-dimensional modelling to precisely capture hydrological processes within green roofs. Using a two-dimensional model allows for simulating water flow and nutrients transport in both vertical and horizontal directions, allowing for a more detailed and realistic representation of flow behavior. Furthermore, two-dimensional models have the capability to portray variations in flow velocity, depth, and direction across space, offering a more thorough comprehension of hydrodynamic processes when compared with one-dimensional models. (Dusek & Vogel, 2014).

5.2.1. Model Properties

In this study, a HYDRUS model utilizing a 2D-general geometry was employed to simulate the hydrological processes within the soil profile. Specifically, the model adopted the 2D-vertical plane XZ domain option to represent the spatial distribution of soil properties and water flow dynamics. The geometry of the model, as shown in Figure 13 featured dimensions of 17.5 cm in depth, 140.17 cm in length, and a 5% slope. Mirroring the composition of the extensive green roof test beds, three distinct sections corresponding to the domain's three layers can also be seen in the figure. This configuration allowed for the accurate representation of the experimental setup.

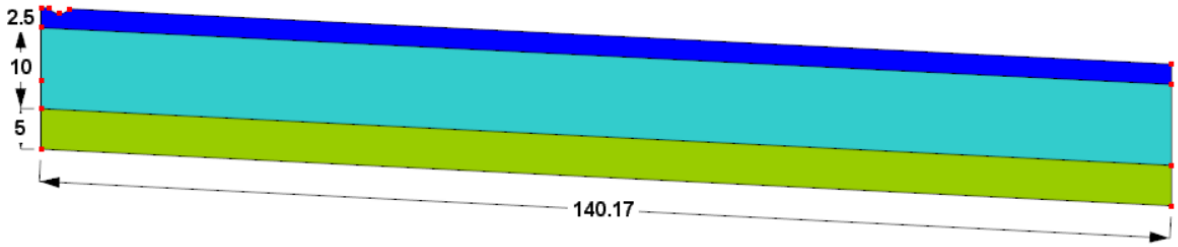

Figure 13 Geometry of the model

To ensure the model accurately simulates the water application pattern and has control over the water input parameters, an arc ditch was defined at the irrigation spot, as shown in Figure 14.

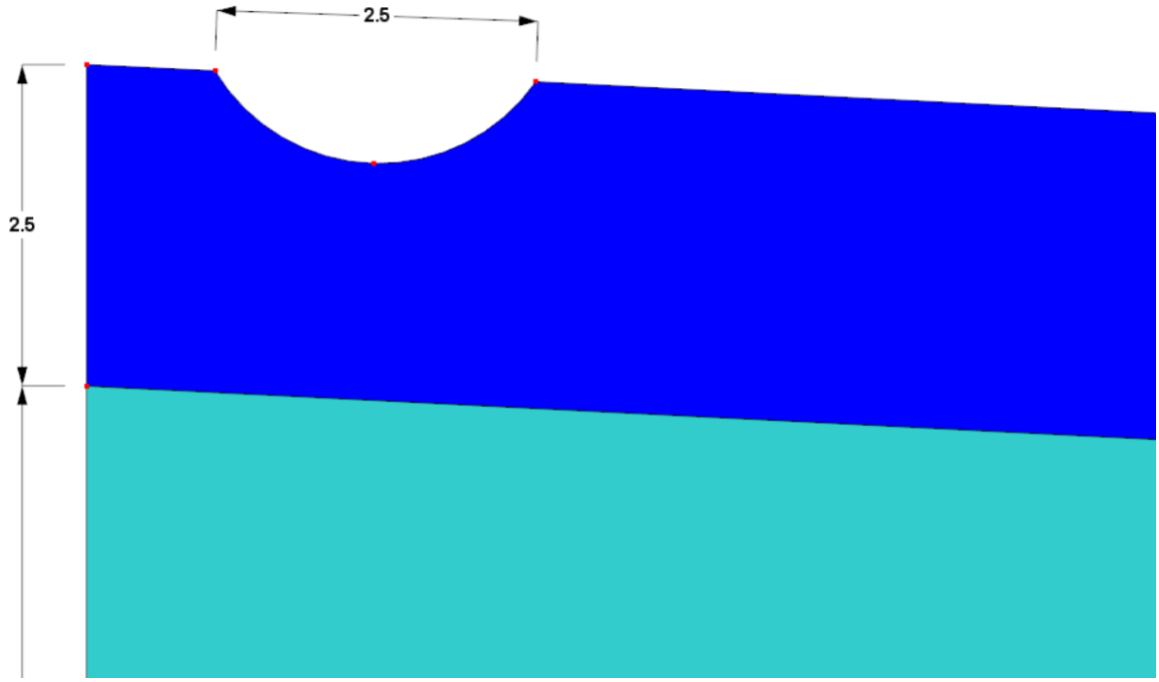

Figure 14 Defined ditch for irrigation application

The profile was discretized into 5915 nodes of 1 cm size by generating a finite-element mesh for the geometry with attention to creating a refined mesh around key areas of interest within the domain. Applying a denser mesh near the region subjected to irrigation application and where seepage face boundary condition was present ensured accurate representation of water movement and distribution in these critical zones with nodes of 0.18 cm. Additionally, finer mesh resolution was implemented at the surface where atmospheric boundary conditions were applied, enabling precise modeling of interactions between the soil and the atmosphere with nodes of 0.58 cm. Figure 16 shows the resulting mesh across the domain and Figure 17 zooms in on the refined area.

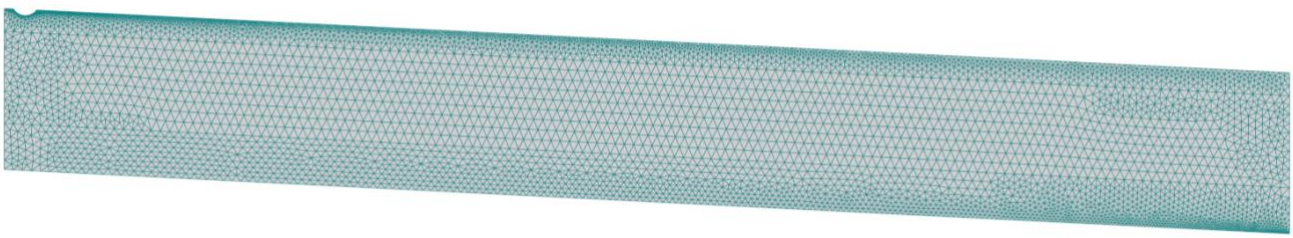

Figure 15 Spatial Discretization of the domain

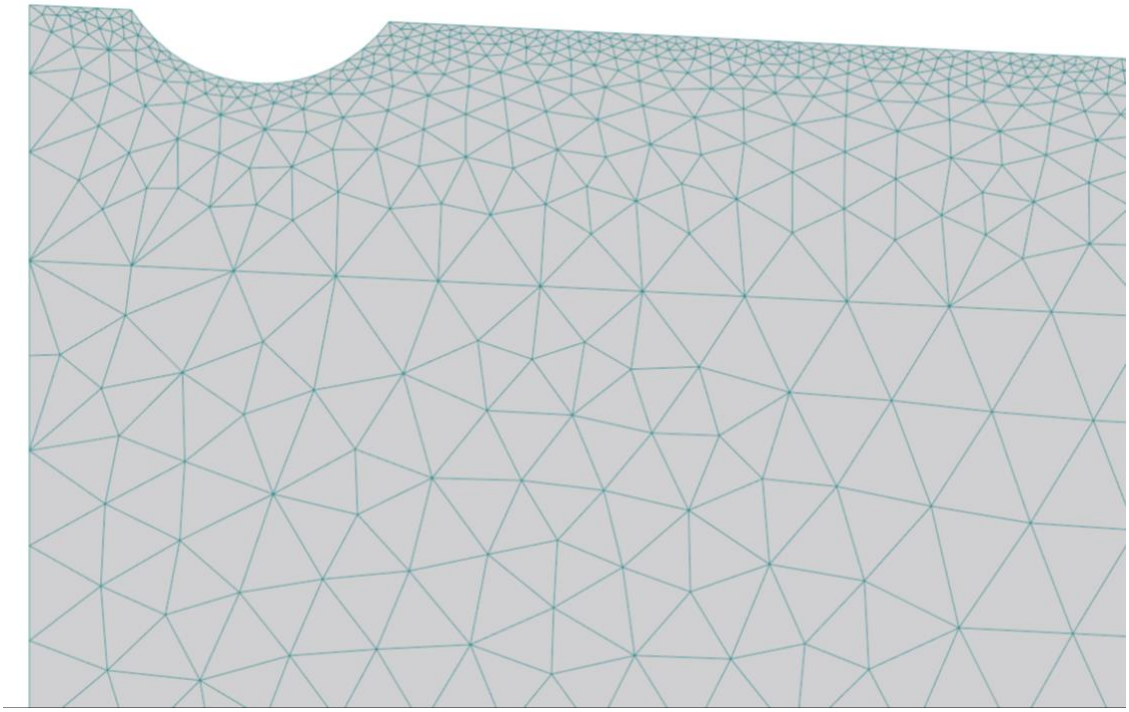

Figure 16 Refined mesh around the ditch

The model was characterized by a precision and resolution level set at 0.00071cm, ensuring accurate representation of variations in water content and pressure head throughout the computational domain. The simulation parameters included a maximum of 100 iterations and a water content tolerance of 0.001.

Run time parameters were carefully defined, with an initial time step and minimum time step both set at 2.4e-005 hr, while the maximum time step was capped at 1 hour. The model operated continuously for a duration of 264 hours, capturing the dynamic hydrological processes unfolding within the simulated green roof system for an 11-day irrigation and monitoring campaign from 18/9/2020 to 28/9/2020.

The hydraulic properties model employed was Van Genuchten-Mualem, with an air-entry value of -2 cm, while no hysteresis effects were considered in the model formulation. These settings facilitated robust simulation of water movement and distribution in the soil profile, providing valuable insights into the hydrological behavior of the studied system. Table 4 shows a summary of all the mentioned properties of the constructed HYDRUS-2D model.

Table 4 Model and water flow parameters

	Property	Value
Domain Type and Units	Type of geometry	2D-General
	2D-Domain Options	Vertical plane XZ
	Length Unit	cm
	Model Precision and Resolution	Epsilon = 0.00071
Time Information	Time Units	Hours
	Initial Time	0
	Final Time	264
	Minimum Time Step	2.4e-005
	Minimum Time Step	2.4e-005
	Maximum Time Step	1
Iteration Criteria	Maximum Number of Iterations	10
	Water content	0.001
	Pressure Head Tolerance	0.5
	Initial Condition	In Pressure Heads
Soil Hydraulic Model	Single Porosity Model	Van Genuchten- Mualem With Air-Entry Value of -2 cm
	Hysteresis	No Hysteresis
Mesh Information	Nodes	5915
	1D-Elements	941 Discretization of Curves (edges)
	2D-Elements	11167 Discretization of Surfaces (faces)
	Boundary Nodes	661
	Boundary Elements	661

The solute transport parameters were then carefully defined. The time weighting scheme employed is the Crank-Nicholson scheme, which balances accuracy and stability by averaging the implicit and explicit methods. For spatial discretization, the Galerkin finite element method is utilized. The simulation considers a single solute with its mass measured in milligrams (mg). These parameters are summarized in Table 5.

Table 5 Solute Transport Parameters

Solute Transport Parameters	Time Weighting Scheme	Crank-Nicholson Scheme
	Space Weighting Scheme	Galerkin Finite Elements
	Number Solutes	1
	Mass Units	mg
	Tortuosity	Millington & Quirk
	Initial Condition	In Liquid Phase Concentrations [Mass_solute/Volume_soil]

Six observation points were strategically placed at various nodes within the flow domain to monitor critical parameters over time. At these observation points, HYDRUS records detailed information about key variables such as pressure head, water retention, temperature, and solute concentration. The nodes are positioned in both the substrate and mineral wool layers: two nodes at the beginning of the domain where water and solutes enter, two in the middle part to observe water distribution and solute degradation across the domain, and two at the end to monitor the final stages of water flow and solute transport. The exact locations of these observation points are clearly presented in Figure 17.

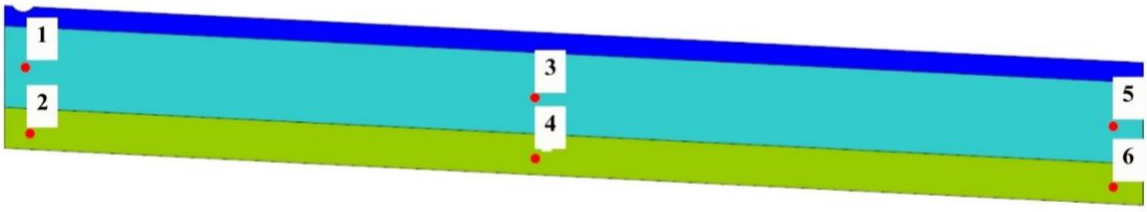

Figure 17 Observation points placements

5.3. Simulating Water Flow

5.3.1. Governing Equation

The governing equation for HYDRUS-2D is the Richards equation (Eq. 1), which describes variably saturated water flow in soils. The model numerically solves the following equation

using a finite element method to simulate water movement in two dimensions (Šimůnek et al., 2016):

$$\frac{\partial \theta}{\partial t} = \frac{\partial}{\partial x}\left[K(h)\frac{\partial h}{\partial x}\right] + \frac{\partial}{\partial z}\left[K(h)\frac{\partial h}{\partial z}\right] - \frac{\partial K(H)}{\partial z} - S(h) \qquad (22)$$

Where θ represents the volumetric water content; h, the matric pressure head (cm); $K(h)$ the soil unsaturated hydraulic conductivity (cm/day); x the horizontal coordinate (cm); z the vertical coordinate (cm); and $S(h)$ the root water uptake term.

5.3.2. Input Data

Material properties:

The material properties inputted into the HYDRUS-2D model for the simulated extensive green roof consist of three layers: Vegetation, Substrate, and Mineral Wool, each contributing to its overall hydrological behavior. The data utilized for these materials, including the volumetric water content (θ_r and θ_s), the van Genuchten parameters (α and n), saturated hydraulic conductivity (K_{sat}), and porosity (represented by *I* to avoid confusion with Van Genuchten's constant, n), were sourced from (Petreje et al., 2023). The Vegetation layer represents the vegetation cover at the surface of the green roof, characterized by a saturated hydraulic conductivity of 5000 cm/hr. The Substrate layer, which lies beneath the vegetation, has similar properties to the Vegetation layer, with a lower saturated hydraulic conductivity of 791.667 cm/hr. Finally, the Mineral Wool layer at the bottom, offering high water retention capabilities has a saturated hydraulic conductivity of 416.667 cm/hr. Table 6 shows the material properties and their layering order can be seen in Figure 18.

Table 6 Materials propertiess

Material		θ_r [-]	θ_s [-]	α[1/cm]	n [-]	K_{sat} [cm/hr]	*I* [-]
1	Vegetation	0.028	0.443	0.84	1.16	5000	0.5
2	Substrate	0.028	0.443	0.84	1.16	791.667	0.5
3	Mineral Wool	0	0.785	0.0509	3.665	416.667	0.5

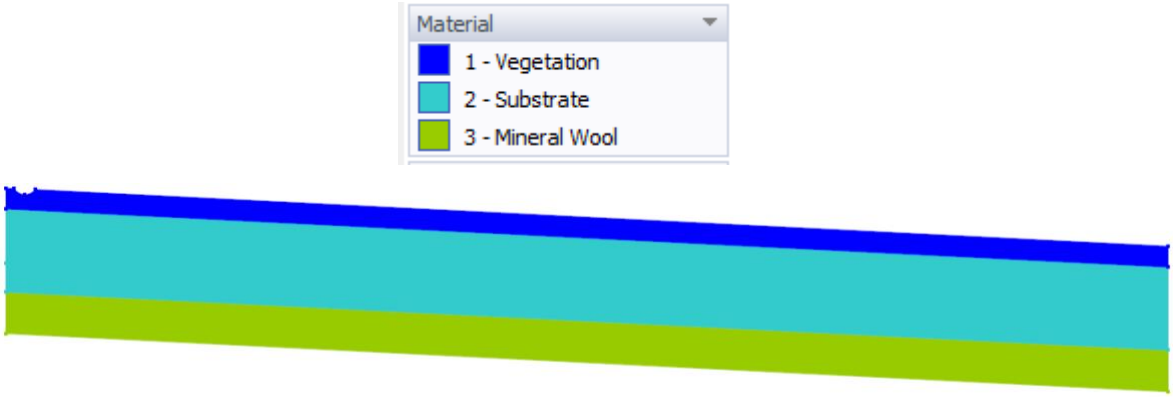

Figure 18 Materials of the domain

Rainfall:

Rainfall data for an the 11-day campaign was extracted from the data recorded by during their experiment. This rainfall data was incorporated into the time-variable boundary condition and applied to the surface with atmospheric boundary conditions. This ensured accurate simulation of the hydrological conditions for the specified period in the Hydrus model.

Evaporation and Transpiration:

Reference evapotranspiration (ET_0) was calculated by (Petreje et al., 2023) using the Penman-Monteith equations, while evaporation rates were determined using the Penman equation. To determine transpiration from ET0, the FAO equation was implemented with the crop coefficient approach (Food and Agriculture Organization of the United Nations, 1998):

$$ET_c = K_c\, ET_0 \qquad (23)$$

where ET_c is crop evapotranspiration, K_c is the crop coefficient, and ET_0 is reference evapotranspiration. K_c used for mixed sedum is 0.56 according to FAO, (1998). The resulting evaporation and transpiration rates which are considered potential evaporation and transpiration are presented in Table 6 and were used as time-variable boundary conditions for the atmospheric boundary at the domain surface.

Table 7 Calculated daily average evaporation, evapotranspiration, and transpiration rates

Date	E [cm/hr]	ET_0 [cm/hr]	T [cm/hr]
9/18/2020	0.010	0.008	0.005
9/19/2020	0.009	0.007	0.005
9/20/2020	0.010	0.008	0.006
9/21/2020	0.012	0.009	0.006
9/22/2020	0.014	0.011	0.008
9/23/2020	0.010	0.008	0.006
9/24/2020	0.011	0.008	0.006
9/25/2020	0.004	0.001	0.002
9/26/2020	0.003	0.002	0.001
9/27/2020	0.003	0.002	0.002
9/28/2020	0.002	0.001	0.001

Evapotranspiration in the model was applied in a simplified way, as an evaporation from the surface. Evapotranspiration values were used as evaporation rates from the green roof and evaporation from the constructed wetland was deducted from the irrigation flux entering the green roof.

Irrigation Flux: In the experiment conducted by (Petreje et al., 2023) 10 liters of greywater were applied daily for 1 minute at 10:00 AM. This irrigation flux first entered the constructed wetland part, where a portion of the water evaporated. The remaining portion of the water then entered the green roof part. Since we are modeling the green roof part only for this modeling project, the inflow into the green roof only is taken into consideration. The path that the greywater flux takes is illustrated in a scheme in Figure 19.

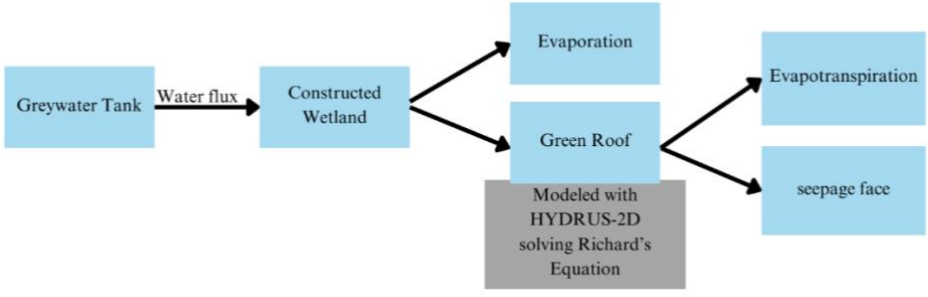

Figure 19 Functional scheme of the path of water in the hybrid green roof system

The 10-liter inflow was adjusted according to the daily evaporation rate from the constructed wetland using the simple equation:

$$Flux\ into\ green\ roof = Flux\ into\ constructed\ wetland - evaporation\ rate$$

resulting in the daily fluxes shown in Table 8. The modified rate was converted from liters per minute to centimeters per hour by applying the flux to the surface area of the irrigation ditch, which measured 2.5x 100 cm². This adjusted flux was then implemented through the time-variable boundary condition to the Variable Flux BC.

Table 8 Irrigation fluxes applied to the variable flux boundary condition

Date	Flux into constructed wetland [L/day]	Evaporation [L/day]	Flux into green roof part [L/m]
9/18/2020	10	2.25	7.74
9/19/2020	10	2.06	7.74
9/20/2020	10	2.31	7.93
9/21/2020	10	2.71	7.68
9/22/2020	10	3.41	7.29
9/23/2020	10	2.68	6.58
9/24/2020	10	2.59	7.32
9/25/2020	10	1.70	7.40
9/26/2020	10	0.98	8.29
9/27/2020	10	1.04	9.01
9/28/2020	10	0.95	8.96

5.3.3. Initial Condition

The initial conditions are pressure head distribution within the soil profile, which is set to achieve equilibrium from the lowest located nodal point bottom upwards. This approach ensures a realistic representation of soil moisture dynamics within the simulation domain.

Initial Pressure Head Value: The pressure head initial condition is set at -7.6 cm in the lowest point of the simulation domain. This value is chosen based on preliminary model calibration efforts. The initial pressure head distribution is presented in Figure 20.

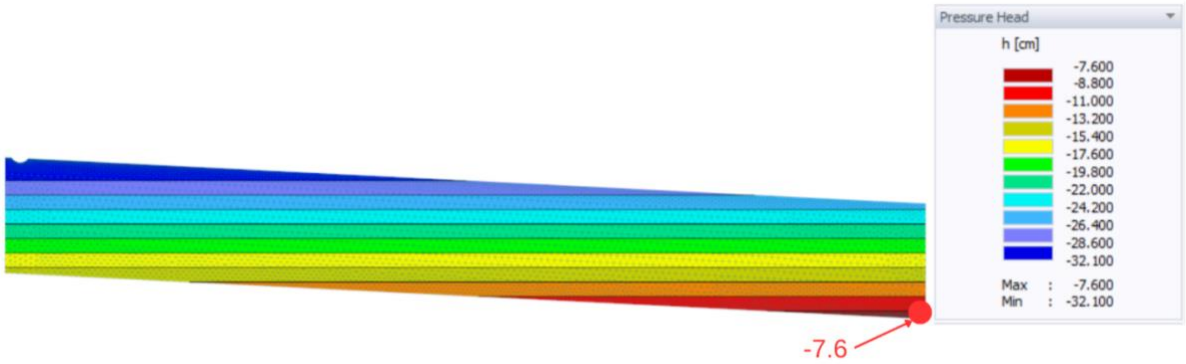

Figure 20 Water flow initial condition in pressure head

5.3.4. Boundary conditions

Diverse boundary conditions are applied to accurately capture the complexities of water movement within the semi – intensive part of hybrid green roof system. At the surface, the atmospheric boundary condition uniformly across the entire simulation domain which includes a time variable boundary condition input of precipitation, evaporation, and transpiration. Additionally, at the top left corner, where irrigation is applied, a Variable Flux boundary condition is employed. This boundary condition adjusts over time to prescribe daily flux inputs of irrigation, through a time-variable boundary condition. At the bottom right corner, representing the outflow boundary, a Seepage Face boundary condition is implemented. This boundary condition simulates the discharge of excess water from the system, reflecting the drainage processes occurring in this region. Along the sides and bottom of the simulation domain, No Flux boundary conditions are implemented, establishing impermeable boundaries where water movement is restricted. The applied boundary conditions are presented in Figure 21.

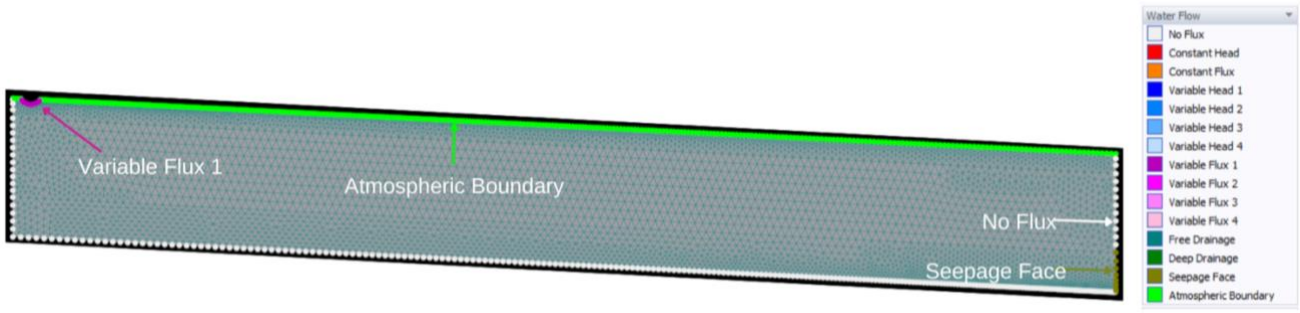

Figure 21 Water flow boundary conditions

In HYDRUS, time-variable boundary conditions are used to simulate changes in boundary conditions over time. Through the time variable boundary conditions table, irrigation flux and solute concentrations were applied to the variable flux boundary condition and precipitation and evaporation were applied to atmospheric boundary condition at the surface. The time variable boundary conditions table can be found in the appendix of this thesis.

5.4. Solute Degradation in Constructed Wetland

The decay of BOD_5 in both horizontal flow (HF) constructed wetland follows first-order kinetics, with rate constants influenced by the design and operational conditions of the wetland beds. The rate of BOD_5 removal is affected by the hydraulic loading rates and the organic load applied to the wetland. Higher pollutant loads generally result in higher mass removal rates, but can also lead to variability in removal efficiency over time (Gajewska et al., 2020).
In the experiment conducted by Petreje et al. (2023), pretreated greywater was used with relatively low levels of BOD_5. However, due to the low frequency of BOD_5 measurements, and high relative error due to low concentrations an assumption was made in this numerical experiment that the irrigation was done with untreated greywater. This assumption is the basis for the calculation of BOD_5 decay in the constructed wetland. The initial BOD_5 of the untreated greywater was chosen to be 80 mg/L. For horizontal flow constructed wetlands, Equation 20 was modified as follows:

$$\frac{C_{out}}{C_{in}} = exp\,(-k_v t) \qquad (24)$$

Where C_{out} in our case is the final BOD_5 at the outlet of the constructed wetland and C_{in} is the initial BOD_5 of the untreated greywater. k_v is the decomposition constant coefficient for BOD_5, which is estimated to be 0.22 by taking an average of the suggested range of 0.15-0.29 by (Gajewska & Ambroch, 2012). t is the hydraulic retention time of BOD_5 and depends on the mean pore velocity and length of the constructed wetland and was found using Equation 23, and mean pore velocity was found using Equation 24.

$$t = \frac{L}{v} \qquad (25)$$

$$v = \frac{q}{n} \qquad (26)$$

Here L is the length of the wetland, v is the mean pore velocity, q is the volumetric flux of the greywater which, and n is the porosity of the medium which was determined in a bachelor thesis by (Mašková, 2022) to be 0.49 for expanded clay.

The final BOD_5 was compared with the initial BOD_5 of untreated greywater to determine the removal efficiency of the wetland. BOD_5 values at different lengths of the constructed wetland were then calculated to observe the plume travel across the wetland, with results presented in section 6.2 of this thesis. The path that solutes take is shown in the scheme in Figure 22.

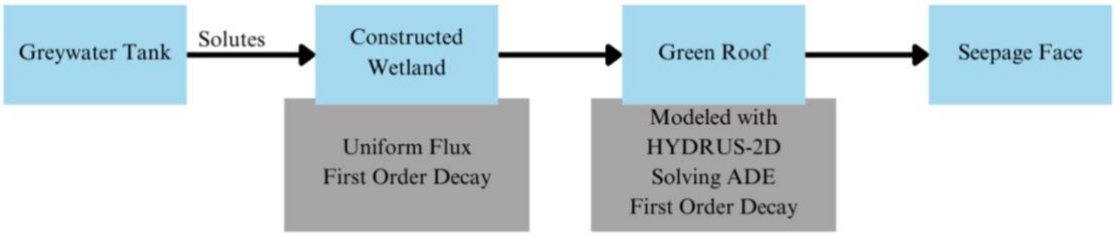

Figure 22 Scheme of solutes transport across the hybrid green roof system

5.5. Simulating Solutes Transport:

5.5.1. Governing Equation

In HYDRUS-2D, the governing equation for solute transport is a form of the advection-dispersion equation, which accounts for the movement and spreading of solutes in a variably saturated porous medium. This equation can be expressed as follows:

$$\frac{\partial(\theta c)}{\partial t} = \frac{\partial}{\partial x}\left(\theta D \frac{\partial c}{\partial x}\right) + \frac{\partial}{\partial z}\left(\theta D \frac{\partial c}{\partial z}\right) - \frac{\partial}{\partial z}(cq) \qquad (27)$$

Where θ is the porosity of the medium, c is the solute concentration, q is water flux density, D is the coefficient of dispersion.

5.5.2. Input data

BOD_5 Calculated in section 5.4 was used as the solute concentration to be injected into the extensive green roof model in HYDRUS. The final BOD_5 at the constructed wetland was calculated to be 16.56 mg/L which was converted to 0.02 mg/cm^3 and applied time variable boundary conditions as shown in Figure 21 in section 5.3.4. Soil specific parameters shown in

Table 9 were then entered. Disp. L represents the longitudinal dispersivity and was estimated using Equation 20 to be 14 cm and transverse dispersivity was assumed to be 10 times smaller than longitudinal dispersivity at 1.4 cm. For this model Diffusion was assumed to be zero.

Table 9 Soil specific transport parameters

Material	Bulk. D. [M/cm^3]	Disp. L. [cm]	Disp. T. [cm]	Fract. [.]	Thlmob. [.]
1	1.5	14	1.4	1	0
2	1.5	14	1.4	1	0
3	1.5	14	1.4	1	0

specific reaction parameters were then defined to simulate the behavior of Biochemical Oxygen Demand (BOD_5) in both dissolved and solid phases. The first-order rate constant for the dissolved phase, denoted in HYDRUS as SinkL1, was set to 0.00916 per hour. Similarly, the first-order rate constant for the solid phase, SinkS1 was also set to 0.00916 per hour. These constants represent the rates at which BOD_5 degrades in the respective phases. Additionally, the decomposition constant coefficient for BOD_5, was determined to be 0.22 per day calculated as the average of the range 0.15 to 0.29 suggested by Gajewska and Ambroch (2012) then converted to 0.00916 per hour.

5.5.3. Initial Condition

The initial condition for the solute concentration, specifically Biochemical Oxygen Demand (BOD_5), were set to zero across the entire flow region. This assumes that the initial state of the domain had no presence of BOD_5, providing a clean baseline for the simulation ensuring that any subsequent changes in BOD_5 concentrations within the domain result solely from the applied irrigation and boundary conditions, rather than pre-existing solute levels.

5.5.4. Boundary Conditions

Solute transport boundary conditions include several types: No Flux (no solute movement across the boundary), First-Type (Dirichlet) which specifies the solute concentration at the boundary, Third-Type (Cauchy or Flux) which prescribes the solute flux and maintains mass balance, and Volatile-Type which permits gaseous diffusion through a stagnant boundary layer above the soil. The Third-Type boundary condition is used at the inlet ditch and seepage face for its ability to accurately control solute flux into the domain, ensuring solute mass conservation. It switches to a Neumann condition when water flux is zero or outward, except for atmospheric boundaries where solutes are assumed not to leave the region (Simunek et al.,

2013). All the other domain boundaries are prescribed with No Flux Boundary conditions. The solute transport boundary conditions are shown in Figure 23.

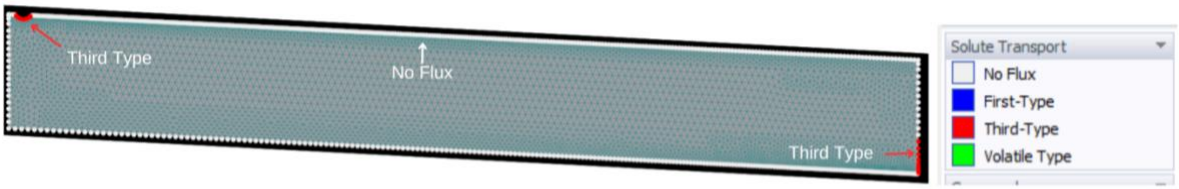

Figure 23 Solute transport boundary conditions

6. RESULTS AND DISCUSSION

The Hydrus 2D model simulations were conducted on HYDRUS 2D/3D version 3, on Windows 10. The total run time for model simulation of an 11-day monitoring campaign was 54.6 minutes, simulating water flow and solute transport at 64910 time levels averaging 2 iterations per each level. Time steps averaged at 0.004 hours, with shorter timesteps applied at times of irrigation and when infiltration is present, as shown in the graph in Figure 24 plotting time steps versus time.

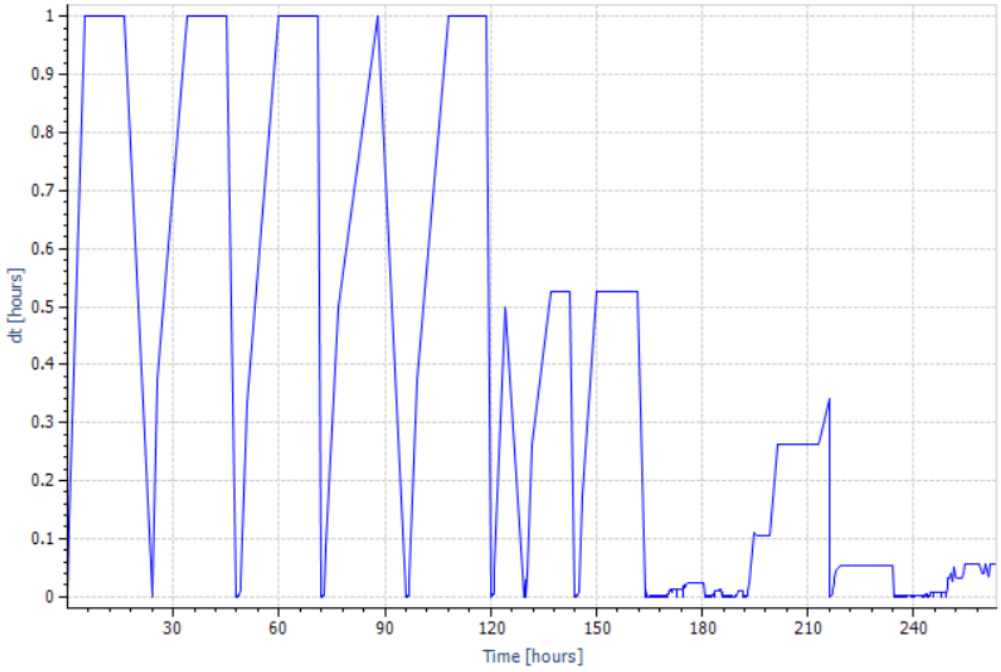

Figure 24 Run Time Information: time vs. time steps

6.1. Water Flow

6.1.1. Water flow direction and velocity vectors

Water enters the domain through two primary pathways. Firstly, through the inlet where irrigation flux is applied, distributing water across the domain as illustrated in Figure 25. Secondly, water infiltrates through the atmospheric boundary, percolating through the vegetation layer and traveling both horizontally and vertically through the substrate layer toward the outlet, known as the seepage face. This process is captured in Figure 26. The seepage face serves as a system-dependent boundary condition where water exits the saturated part of the flow domain, also can be observed in Figure 26. Additionally, water leaves the domain through evaporation across the atmospheric boundary, as shown in Figure 27.

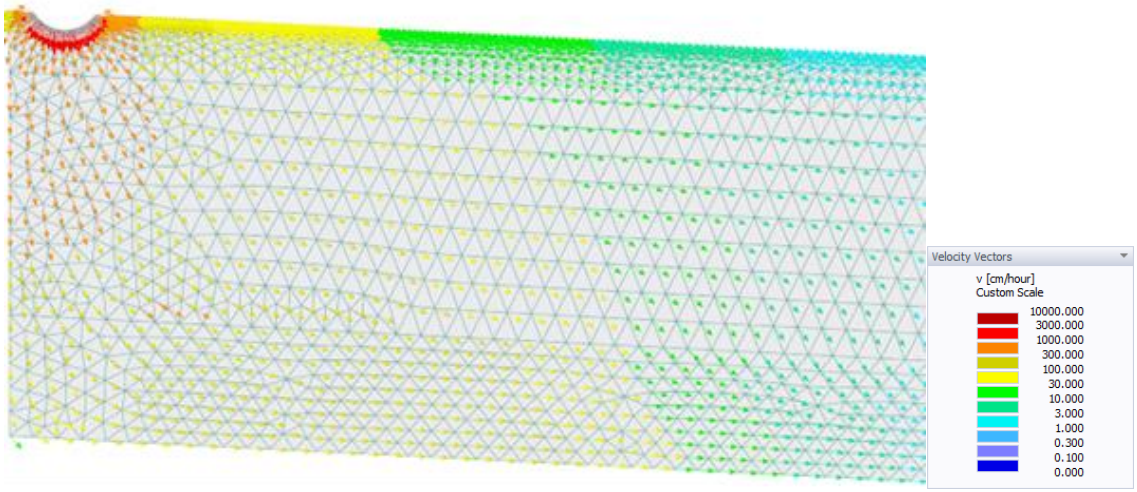

Figure 25 Velocity vectors of water flow during the first irrigation pulse at 0.01 hours, on a 40-cm section

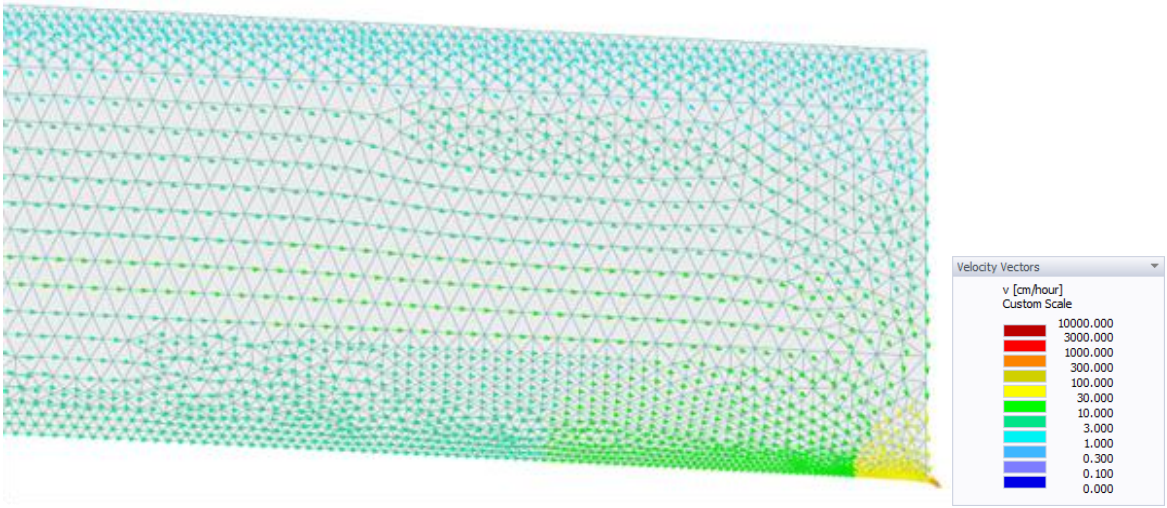

Figure 26 velocity vectors of water flow during a rainfall event at 156 hours, on a 40-cm section

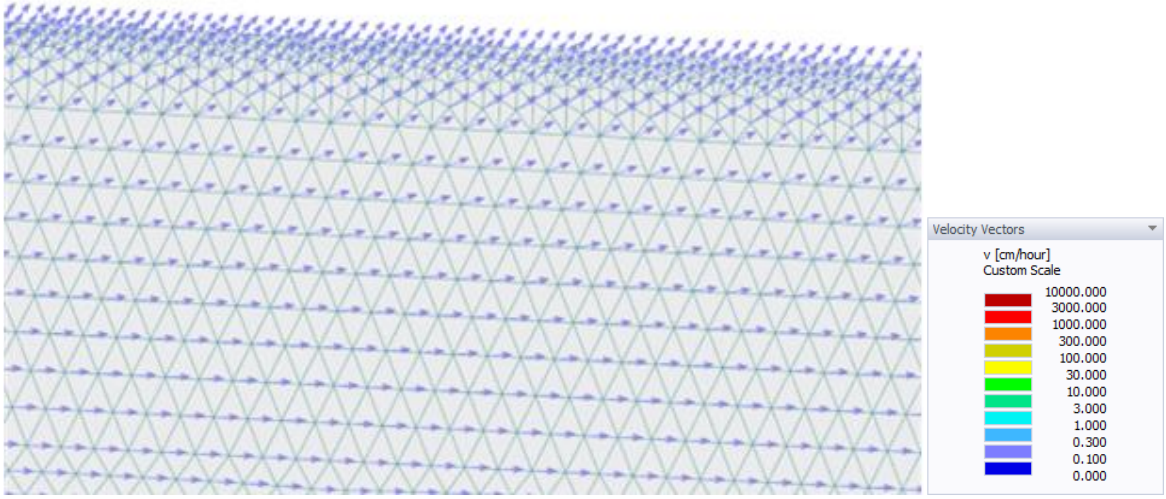

Figure 27 Velocity vectors of water flow during evaporation at 97 hours, on a 30-cm section

The output from HYDRUS, as shown in Figure 28, illustrates the spatial distribution of water content at four different time steps during a single irrigation pulse: 0.0001 hours, 0.001 hours, 0.01 hours, and 0.1 hours. These images show how water infiltrates and distributes through the green roof over time, influenced by high hydraulic conductivity which allows water to move downwards quickly. At the very beginning of the irrigation event, water content is higher near the inlet ditch where irrigation is applied than the other parts of the surface, with the increased water content localized to the uppermost layer. Shortly after irrigation begins, water continues to infiltrate, spreading laterally and slightly deeper into the substrate layer and showing initial signs of downward percolation at the interface between the substrate and mineral wool layers. As irrigation progresses, water infiltrates deeper into the soil profile, moving downwards rapidly due to high hydraulic conductivity, leading to quick saturation of deeper layers.

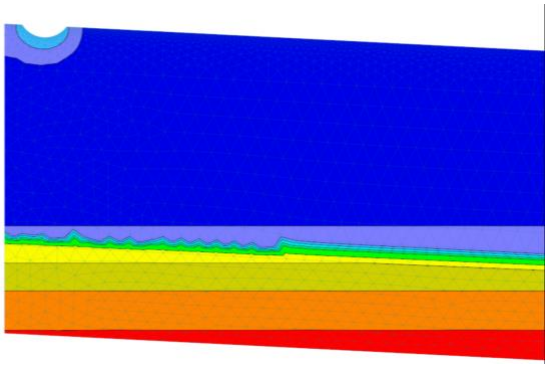

a) water content at time 0.0001 Hour

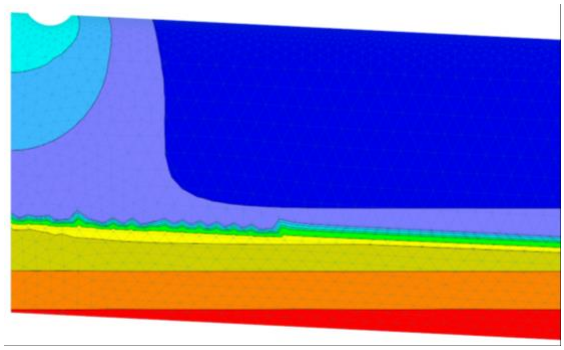

b) water content at time 0.001 Hour

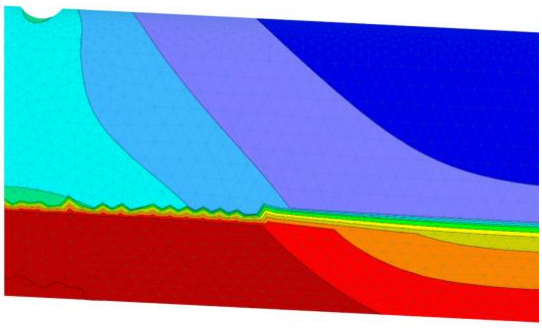

c) water content at time 0.01 Hour

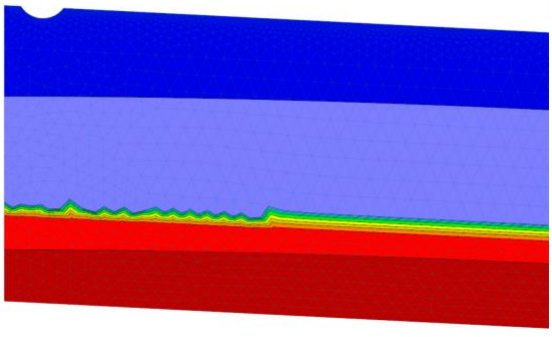

d) water content at time 0.1 Hour

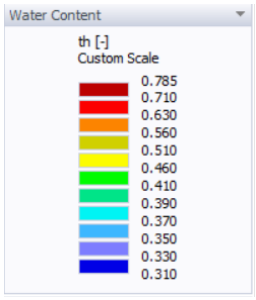

Figure 25 Water Content distribution during a single irrigation pulse at 4 different times

The following two images illustrate the water content distribution at the initial time (Figure 29) and the final time after 11 days of daily irrigation and multiple rainfall events (Figure 30). At the initial time, the domain shows a distinct stratification of water content due to material properties of layers.The surface and upper layers exhibit low water content, represented by dark blue and lighter blue hues.

Deeper layers, especially towards the bottom, have higher water content, indicated by red and orange colors. After 11 days of daily irrigation and multiple rainfall events, the water content distribution has significantly changed. The surface and upper layers show much higher water content, transitioning from blue to lighter blue and even to red in some areas.

The deeper layers remain saturated, but there is a more uniform water content distribution across the entire domain. The increased water content throughout the profile reflects the cumulative effect of continuous irrigation and rainfall, resulting in overall higher soil moisture levels and less pronounced stratification compared to the initial state.

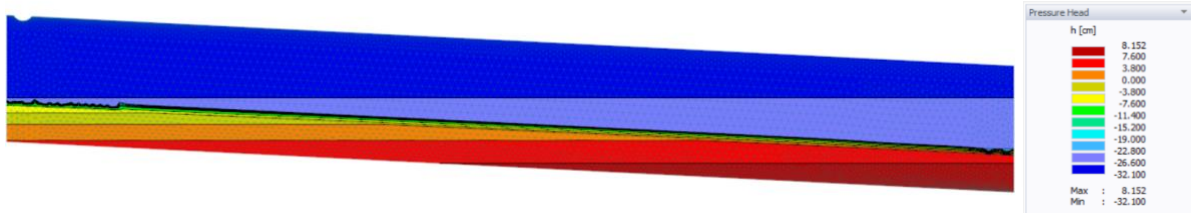

Figure 26 Water content at time 0

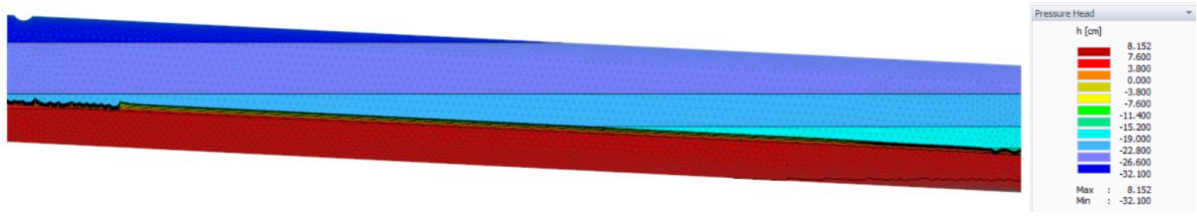

Figure 27 Water content at final time

6.1.2. Pressure Heads

These water distributions and flow dynamics depend on pressure head variations. Specifically, we examine pressure heads at the beginning and end of the flow domain, recorded at observation points 2 and 6. These points are located at the bottom of the domain at the same

soil depth, with point 2 at the beginning of the flow domain and point 6 positioned closer to the seepage face. The exact locations of these observation points are presented in Figure 17. The comparison between these two positions is plotted in Figure 31 where significant difference in the pressure head can be observed. As the initial conditions were set in pressure heads to be -7.6 cm at the lowest point, which is at the seepage face, pressure head at observation point 1 starts at a lower pressure head value and exhibits fluctuations over time, while at observation point 2 begins at a higher value with less variability.

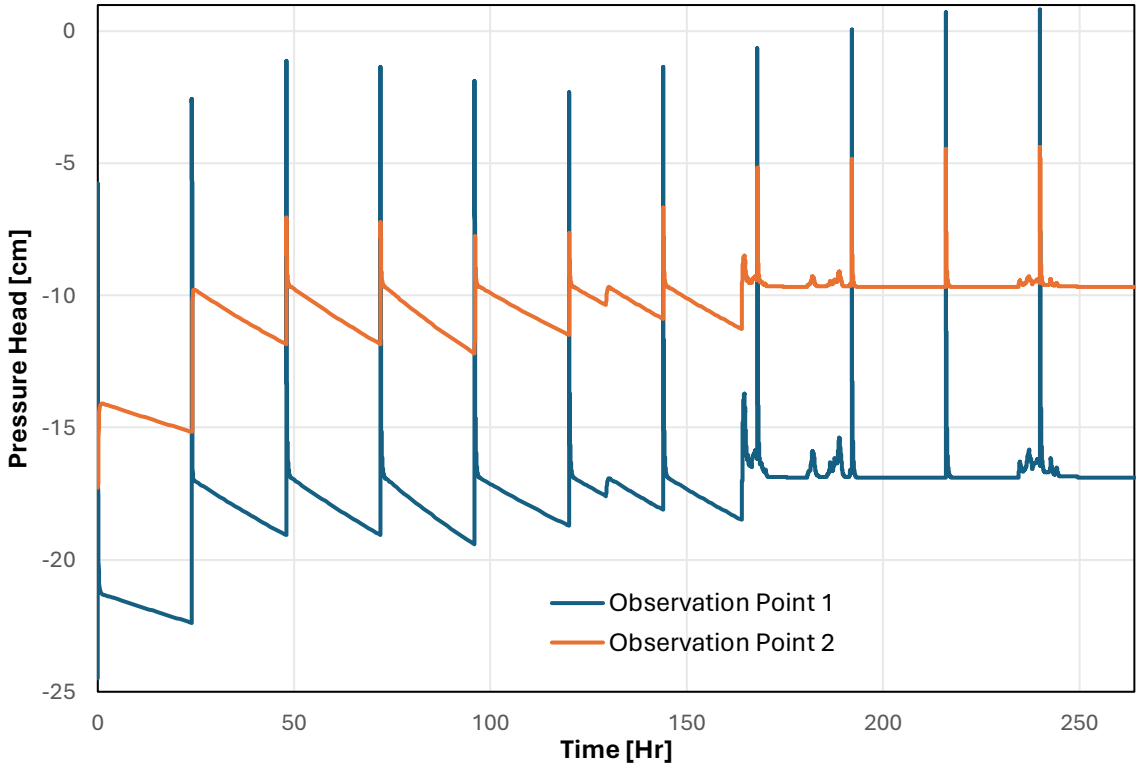

Figure 28 Pressure heads at different positions on the flow domain

The distribution of pressure head is visualized at three different times to provide a comprehensive view of its evolution over time. Figure 32 shows the initial condition before any water flux is applied, showing an equilibrium from the lowest node, which serves as a reference point for understanding the changes. Figure 33 shows the pressure head distribution at 0.01 hours, representing the system's response to the first pulse of irrigation. At this stage, the introduction of water flux causes an immediate increase in pressure head, especially near the surface, indicating the start of water infiltration and redistribution through the soil profile. Figure 34 shows the pressure head distribution at 264 hours, after 11 days of daily irrigation and multiple rainfall events. By this time, the pressure head has increased throughout the soil

profile, with the lowest node having a pressure head of -0.003 cm reflecting the cumulative impact of continuous water application and a more uniform gradient compared to the initial and early stages.

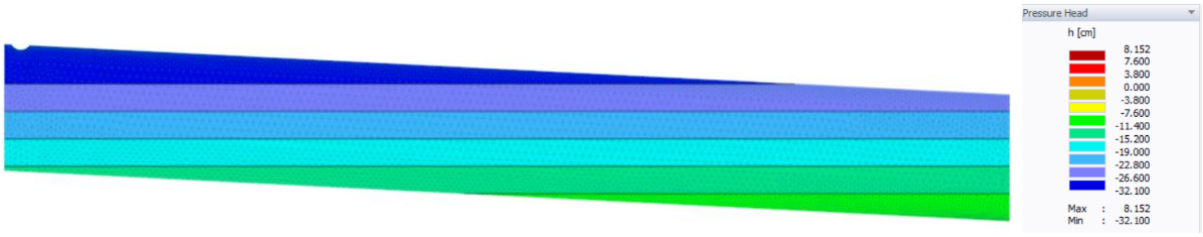

Figure 29 Initial pressure head distribution

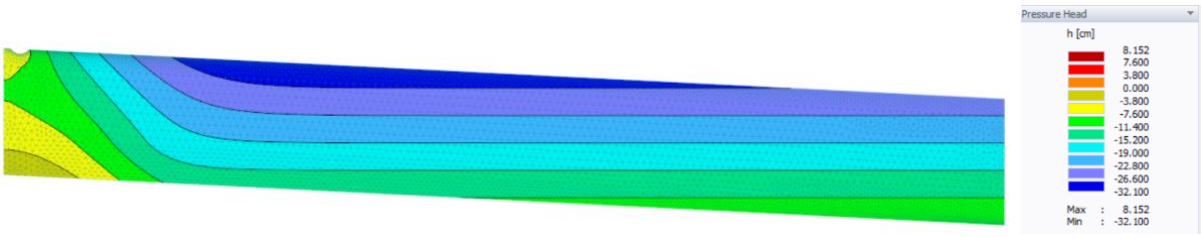

Figure 30 Pressure head distributions at 0.01 hours

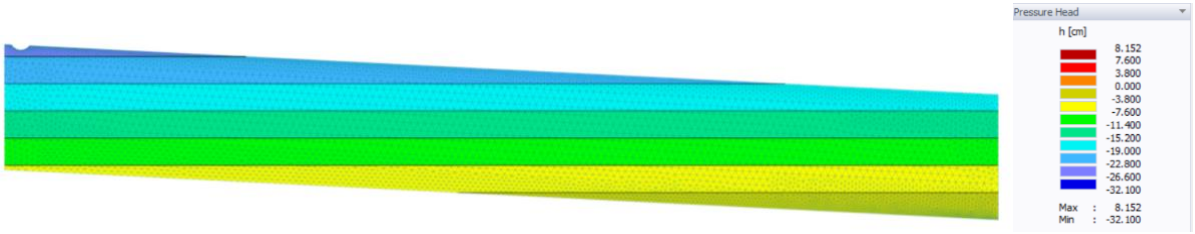

Figure 31 Pressure head distributions at 264 hours

6.1.3. Water Fluxes at Boundaries

The cumulative fluxes across the boundaries are plotted in Figure 35 where the x-axis represents time in hours, while the y-axis shows the cumulative fluxes in liters. *Var. Fl 1* (red line) represents the variable flux of irrigation each step corresponding to a pulse of greywater. The total cumulative flux reaches 89.1 liters by the end of the simulation period. Infiltration (blue line) represents the cumulative water infiltrating into the green roof substrate during rainfall events the total infiltration reaching 61.2 liters. Seepage Face Flux (green line) shows the cumulative flux through the seepage face, which is the boundary where water exits the system. The stepwise rise up to the sixth day represents the outflow of the irrigation water with a delay of close to 24 hours, after rainfall events start, the stepwise increase disappears, and

outflow represents both irrigation and rainfall leaving the system culminating in a total flux of 121.8 liters. Evaporation (Blue Line) indicates the cumulative water loss due to evaporation. The gradual increase reflects the continuous process of evaporation, reaching a cumulative total of 20.7 liters over the simulation period.

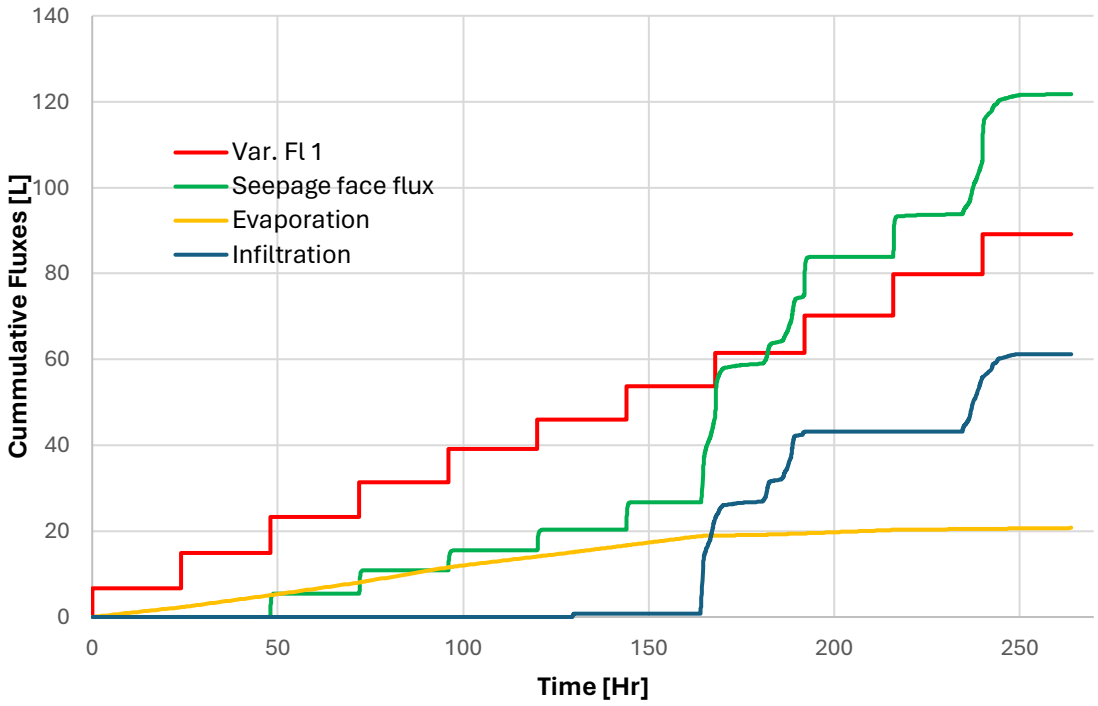

Figure 32 Cumulative fluxes of the model at the boundaries of the domain showing inflow through irrigation, infiltration of rainfall, evaporation, and outflow through seepage face

These fluxes were then compared with the measured data from the experiment by (Petreje et al., 2022), the measured cumulative fluxes are plotted in Figure 36. Both graphs show a stepwise increase in inflow, corresponding to the irrigation events and the irrigation pulses are clearly defined in both the modeled measured data. However, the measured inflow represents the water entering the constructed wetland part which is the total daily irrigation and a total of 111 liters. While in the HYDRUS model only the portion of inflow is modeled that enters the green roof.

Measured precipitation and modelled infiltration values are similar indicating accurate rainfall simulation. Both datasets of calculated evaporation from the experiment and the evaporation from the model exhibit a continuous and gradual increase in cumulative evaporation. However, the calculated combination of evaporation and evapotranspiration from the experiment totals

43.5 liters, more than double the modeled evaporation of 20.7 liters. This significant difference suggests that the model may underestimate evapotranspiration processes. This was because of different method of evapotranspiration calculation was used in this study than by Petreje et al. and because the evapotranspiration was in simplified way applied as evaporation to the surface of the soil without involving the transpiration from defined root zone. Therefore, further efforts are needed to accurately simulate both evaporation and transpiration rates for this specific project.

Both datasets show an initial stepwise increase in outflow, indicating the outflow primarily due to irrigation. After the start of rainfall, both datasets show a continuous increase in outflow, reflecting a mix of irrigation and rainfall exiting the system. However, the total outflow amount is less than the modeled outflow flux at a total of 84 liters. because of the evaporation differences.

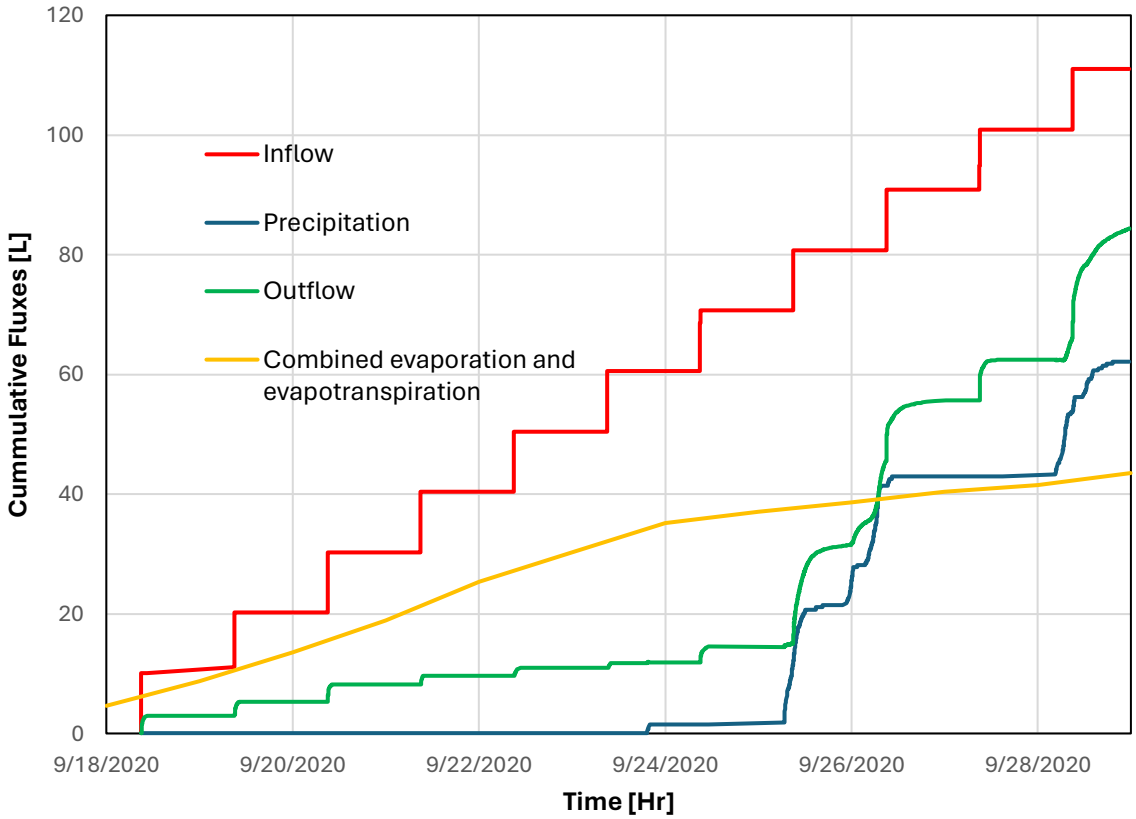

Figure 33 Measured Cumulative fluxes (adapted from Petreje et al. 2023)

The results of the modeling are reliable only when calculated water balance error stays small. This can be challenging at some circumstances The water balance performed by the model resulted in an error of 1.9%, which indicates the degree of discrepancy between the amount of water entering and leaving the system and the changes in water storage within the model during

the simulation. Generally, the goal is for error level to be below 1%, but given the challenging conditions of high fluxes of irrigation, high saturation, and highly conductive materials the error level is satisfactory. This reasonable level of error was achieved through the careful selection of iteration criteria and adjustments in spatial discretization. Additionally, unnecessary timestep creation due to time-variable boundary conditions was avoided by limiting the input of variable fluxes to only three specific timesteps per irrigation pulse. It was realized during the modeling process that more timesteps in variable boundary conditions lead to higher error percentages.

6.2. BOD_5 Removal in Constructed Wetland

The resulting BOD_5 at the outlet of the constructed wetland was calculated to be 16.56 mg/L, which gives the constructed wetland a BOD_5 removal efficiency of 79%. This result is in good agreement with results from extensive surveys evaluating the cleaning efficiency of constructed wetlands with horizontal water flow through root filters. These studies indicate an average BOD_5 removal efficiency of 85%, with a range between 65% and 95% (Šálek et al., 2013). Figure 37 shows the exponential decay of BOD_5 across the length of the constructed wetland.

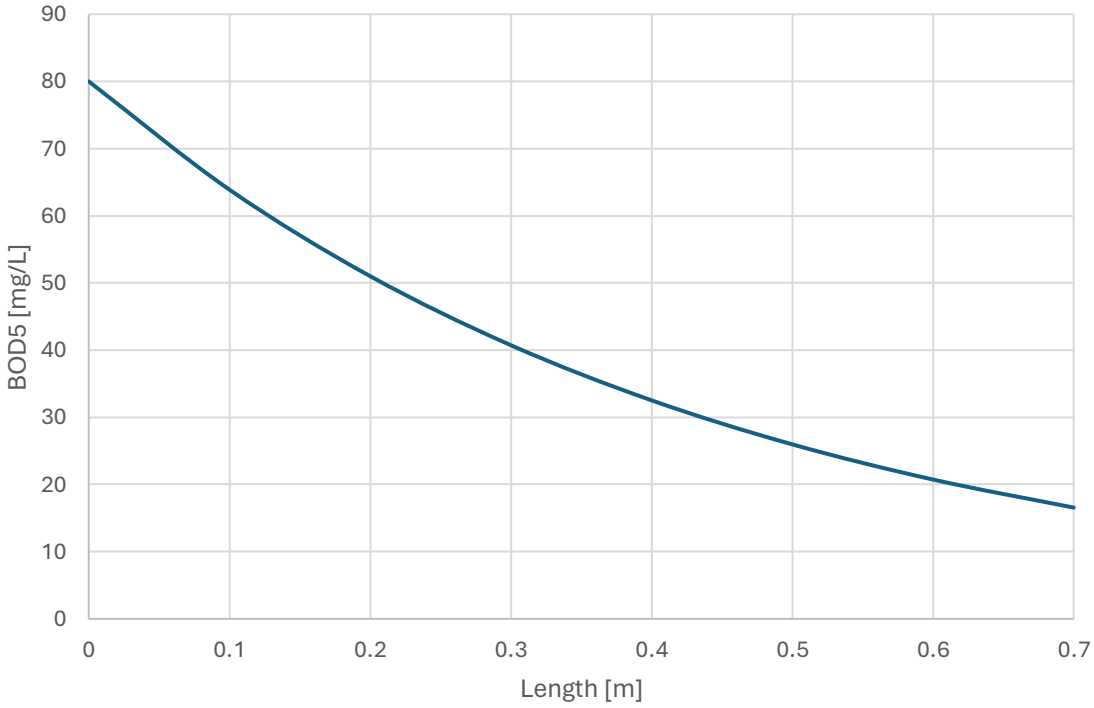

Figure 34 BOD_5 decay along the length of the constructed wetland

6.3. Results of solute transport modeling in semi intensive green roof using HYDRUS

Levels of BOD_5 at the initial pulse of solute injection as it enters the flow domain and begins to disperse both horizontally across the green roof and vertically through the soil layers are represented in Figure 38 using color gradients to represent the concentration. The highest concentration is observed near the inlet, with colors transitioning from yellow to dark blue, indicating decreasing concentrations as the solute moves further from the source.

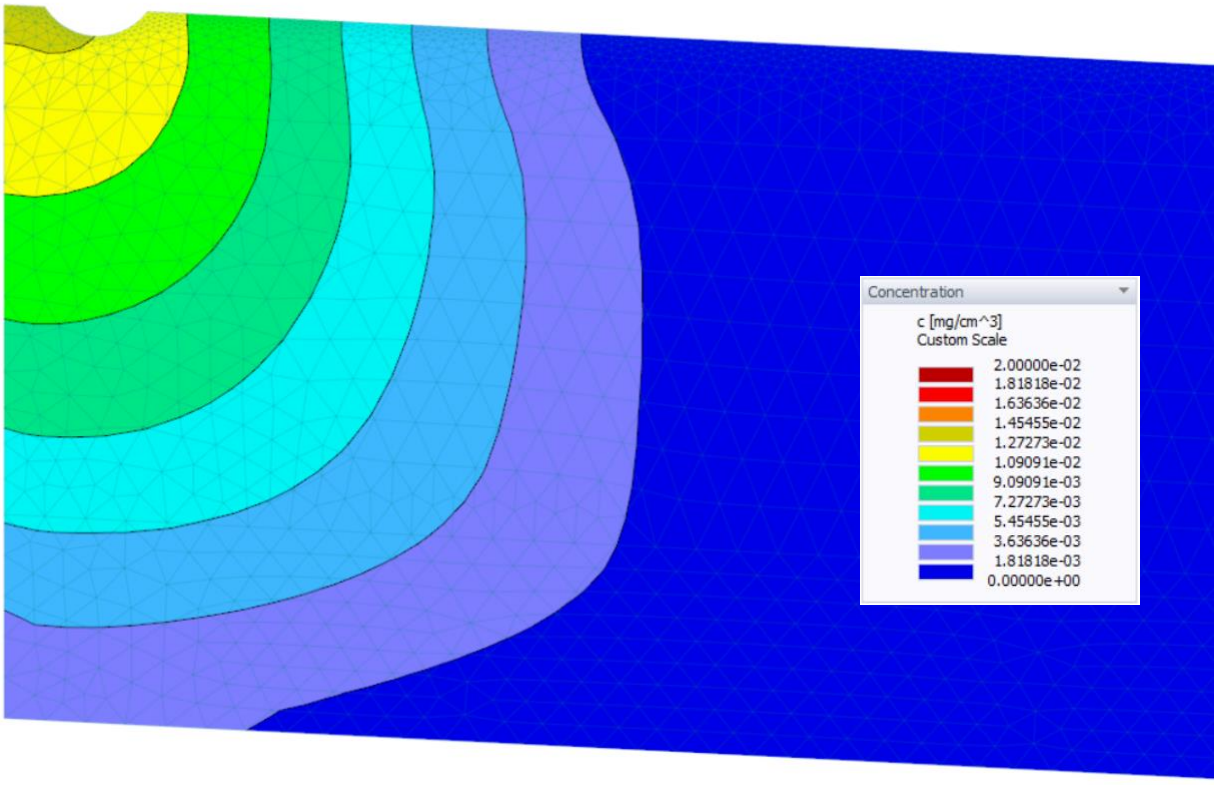

Figure 35 Solute Concentration (BOD_5) entering the domain at the first pulse on a 30-cm section

Initially, the model was run without incorporating solute degradation processes. This scenario aimed to provide a baseline understanding of the solute's physical transport mechanisms solely through advection and dispersion. Figure 39 illustrates the BOD_5 distribution across the green roof at the end of the simulation period. Without degradation, the solute, initially introduced from the irrigation ditch, spreads extensively through the flow domain. In this scenario, a significant concentration of the solute persists across the entire green roof towards the outlet of the flow domain.

To evaluate the influence of degradation on solute transport, the model was then run with degradation processes enabled. Figure 40 presents the results of this simulation. The inclusion

of degradation shows a marked decrease in solute concentration throughout the flow domain and particularly at the outlet, illustrating the effectiveness of the green roof's processes in reducing BOD_5 as water traverses the green roof.

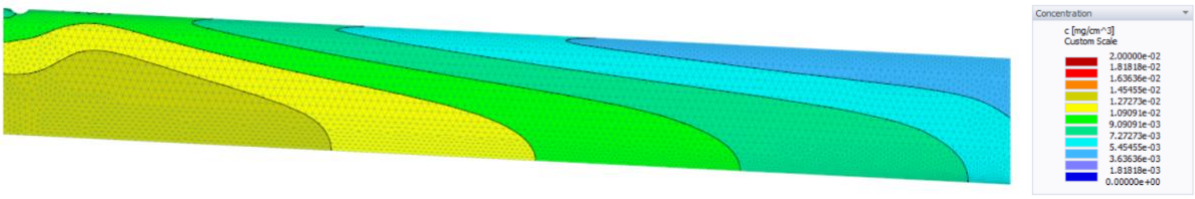

Figure 36 BOD_5 at the end of simulation period, without degradation

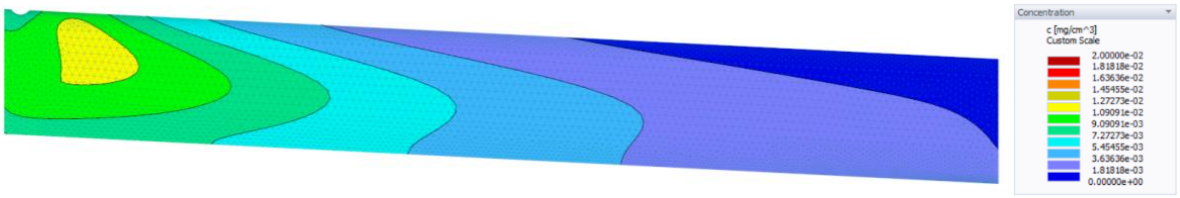

Figure 37 BOD_5 at the end of simulation period, with degradation

The solute balance for BOD_5 was performed by comparing the cumulative inflow and outflow over time. Figure 41 plots a visual representation of the cumulative amounts of BOD_5 entering and exiting the system over a period of 11 days in two different scenarios. The "Solute Influx" line represents the cumulative BOD_5 inflow, showing a stepwise increase indicating periodic pulses added with irrigation pulses, reaching approximately 15.45 mg/cm by the end of the observation period. "Seepage Face (without degradation)" line represents the cumulative solute outflows when degradation is not considered reaching 4.8 mg/cm, and the "Seepage Face (without degradation)" line, representing the cumulative solute outflow, shows a much slower and more gradual increase, reaching only about 1.27 mg/cm and starting significantly later than the inflow. This indicates effective degradation of BOD_5 within the system, with the majority of the solute being retained and broken down before exiting. The system ultimately achieves a solute balance where the input, output, and breakdown rates align, resulting in a mass balance error of just 2%. This minor error is likely due to the spatial discretization and meh refinement, which can be improved in future studies.

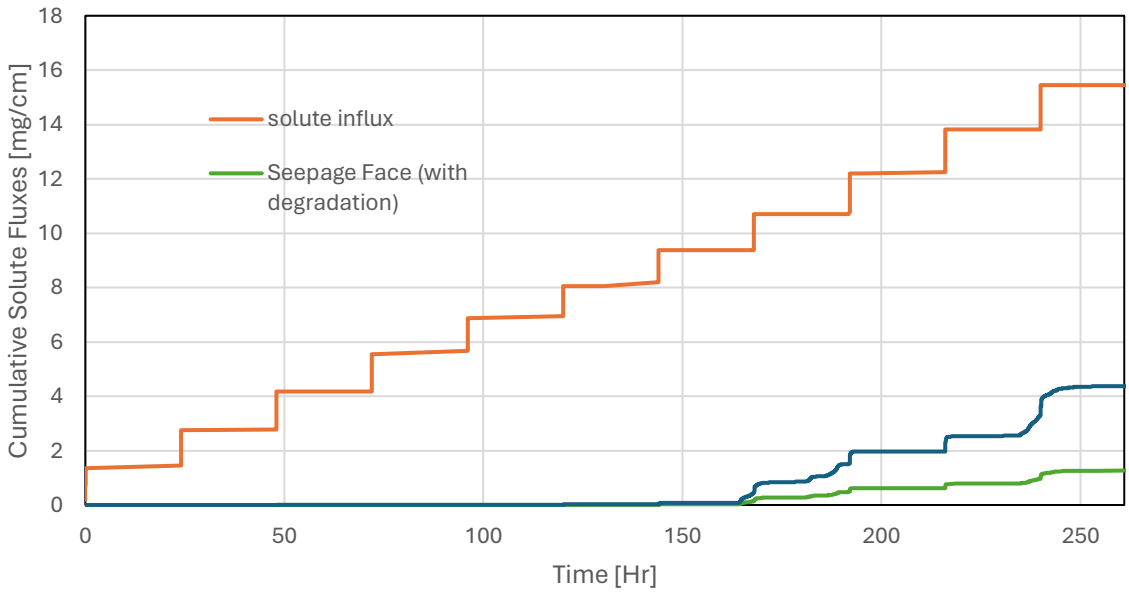

Figure 38 Cumulative solute fluxes

The results BOD_5 recorded at each observation point was exported and plotted in the graphs shown in Figure 42 illustrating the temporal variation in BOD_5 levels at different locations within the domain, capturing the dynamics of solute transport and degradation from the point of entry through the middle of the domain to the exit points with time on the x-axis and BOD_5 on the y-axis.

Observation Point 1 and Observation Point 2 show the BOD_5 levels at the beginning of the domain where solutes enter. The cyclic pattern indicates periodic influxes of solutes corresponding to irrigation events. BOD_5 levels rise sharply with each influx and then decrease as the solutes are transported further into the domain and degraded over time.

Observation Point 3 and Observation Point 4 located in the middle part of the domain, these graphs show a rising trend in BOD_5 levels over time, reflecting the continued input and partial degradation of solutes. When compared to Observation Points 1 and 2, the peaks reach lower heights, indicating the effect of degradation as the solutes move through the domain.

Observation Point 5 and Observation Point 6 represent the final stages of solute transport in the domain. The BOD_5 levels here show lower overall values compared to the initial and middle points, indicating significant degradation and dispersion of solutes as they travel through the domain.

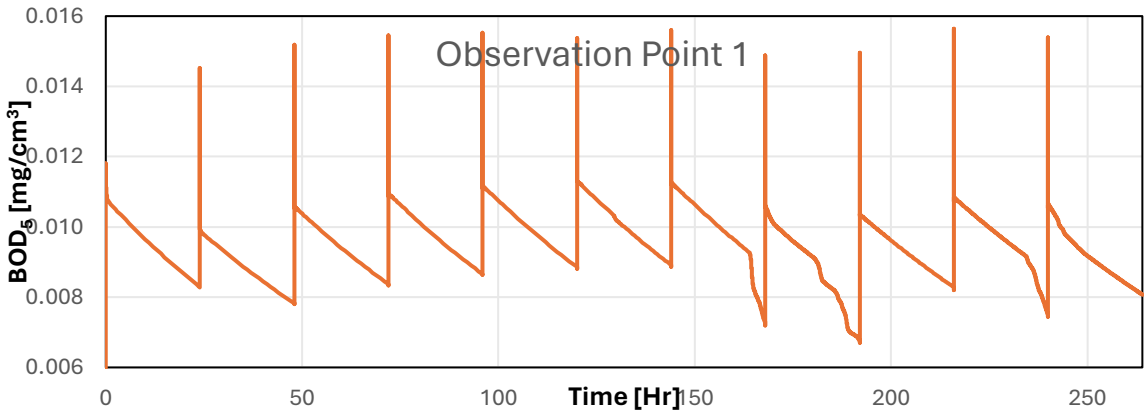
Observation Point 1
BOD5 [mg/cm3]
0.016
0.014
0.012
0.010
0.008
0.006
0
50
100
150
200
250
Time [Hr]

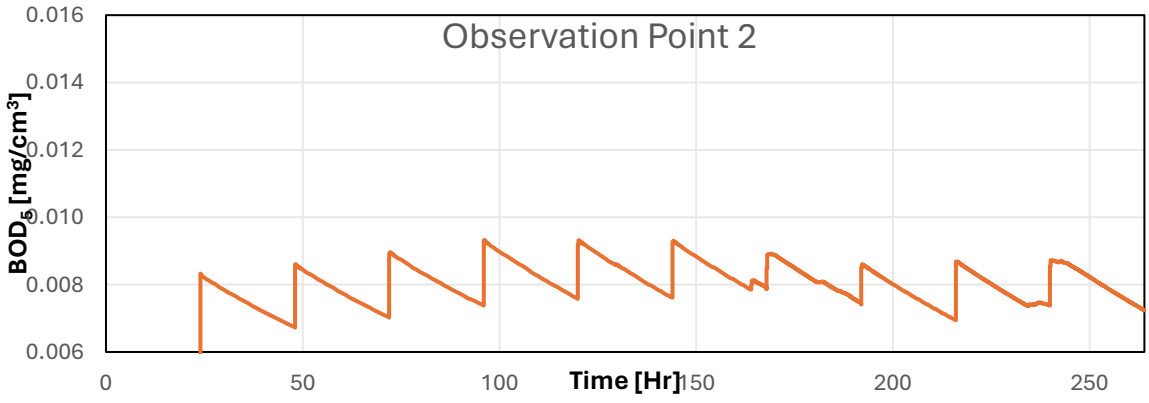
Observation Point 2
BOD5 [mg/cm3]
0.016
0.014
0.012
0.010
0.008
0.006
0
50
100
150
200
250
Time [Hr]

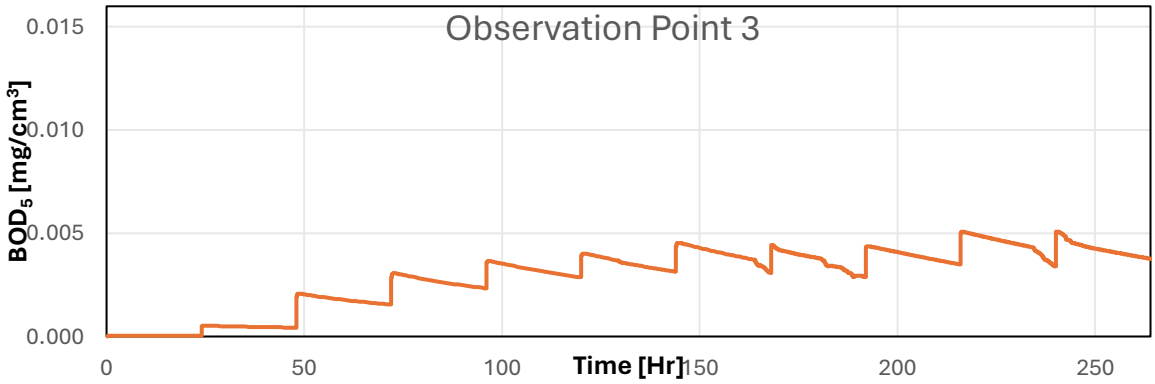
Observation Point 3
BOD5 [mg/cm3]
0.015
0.010
0.005
0.000
0
50
100
150
200
250
Time [Hr]

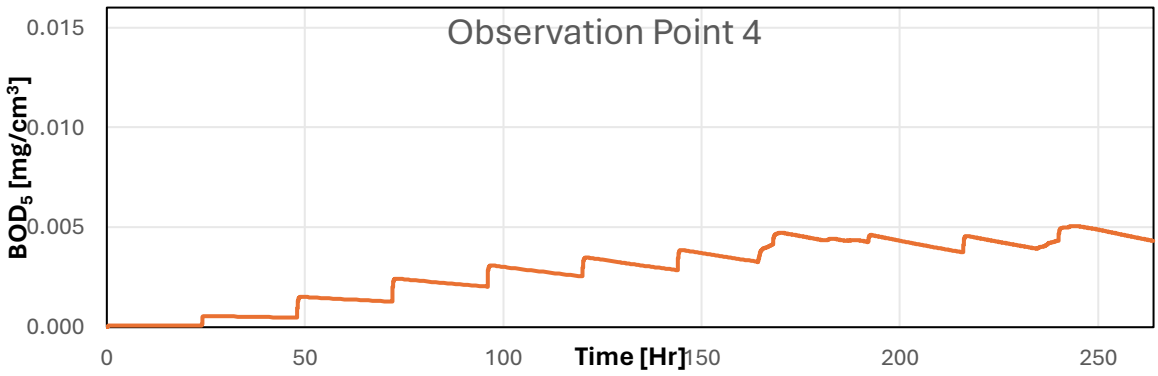
Observation Point 4
BOD5 [mg/cm3]
0.015
0.010
0.005
0.000
0
50
100
150
200
250
Time [Hr]

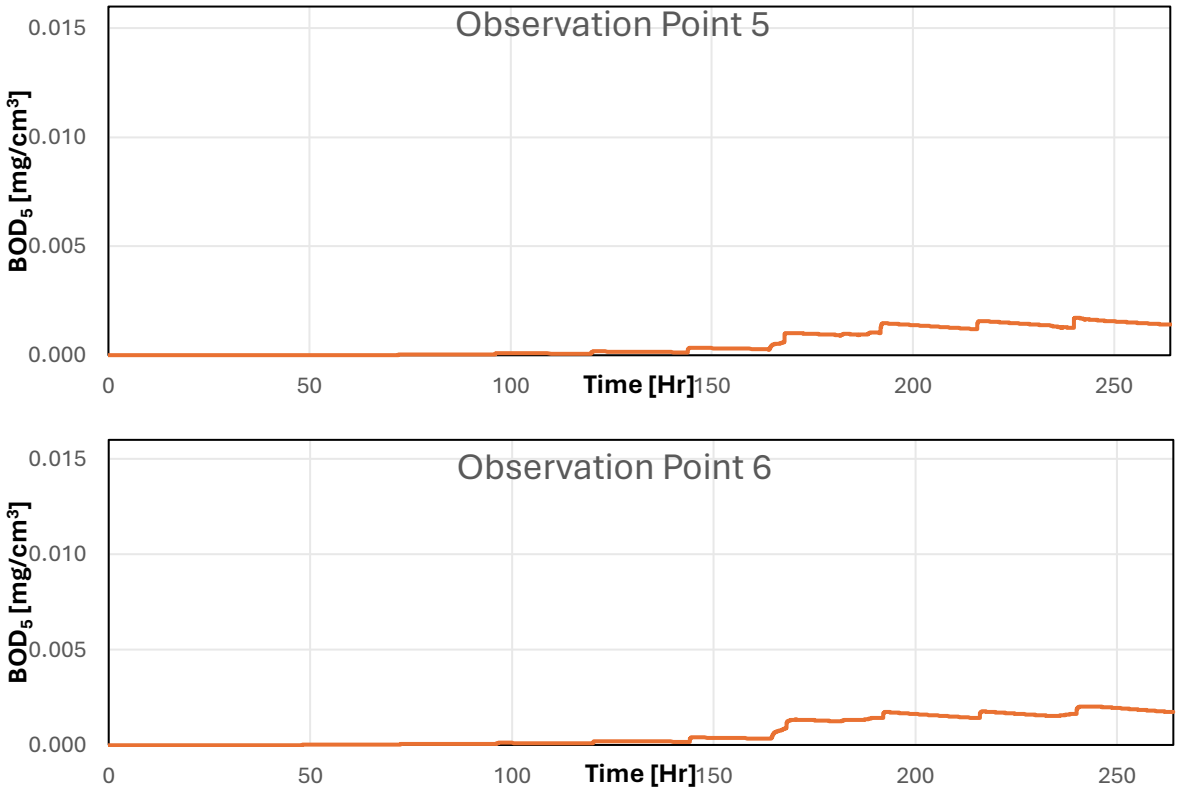

Figure 39 BOD_5 at six observation points across the domain

7. CONCLUSION

This thesis demonstrates the potential of a hybrid green roof system that integrates a constructed wetland with a semi-intensive green roof. The primary objectives were to model water flow and solute transport using the HYDRUS-2D software, interpret measured data, build a digital twin for an existing hybrid green roof, and explore the impact of applying solute loads on the system's performance.

The development of the conceptual model and subsequent numerical simulations using HYDRUS-2D provided valuable insights into the dynamics of water and solutes movement within the hybrid system.

Key findings from the simulations include:

- **Water Flow and Distribution:** The model simulates water low directions and water content distribution accurately, reflecting pressure head variations and hydraulic properties of the domain. Boundary fluxes were compared with measured data and mostly showed good agreement, but the model underestimated cumulative evaporation fluxes and overestimated cumulative outflow from the system.
- **Mass Balance Errors:** High fluxes of irrigation and high hydraulic conductivity of the domain cause high levels of mass balance error at 2%, and require careful selection of iteration criteria and spatial discretization.
- **Solute Transport and Fate:** The model shows that the hybrid system effectively degrades solutes, such as BOD5, demonstrating a marked decrease in concentration from the point of entry to the exit. The constructed wetland has a BOD_5 removal efficiency of 79% and degradation in the semi-intensive green roof is evident when degradation processes are enabled in the simulations, highlighting the green roof's ability to reduce solute loads before water exits the green roof by 3.6 milligrams for each cm of water in the 2D domain.

In conclusion, this thesis confirms the significant potential of hybrid green roofs in advancing sustainable urban water management. By combining the strengths of constructed wetlands and green roofs, these systems offer a promising approach to addressing contemporary environmental challenges in urban areas. The results of this study contribute to the field of environmental engineering by offering a simplified digital twin of the hybrid green roof system that can be used for further research and practical. Future research should focus on long-term monitoring of hybrid green roof systems in real-world settings to validate and refine the model

further. Additionally, exploring modeling of the integration of other eco-technologies and the use of recycled materials in green roof substrates could enhance the sustainability and performance of such system.

REFERENCS

Albalawneh, A., & Chang, T.-K. (2015). REVIEW OF THE GREYWATER AND PROPOSED GREYWATER RECYCLING SCHEME FOR AGRICULTURAL IRRIGATION REUSES. *International Journal of Research -GRANTHAALAYAH*, *3*(12), 16–35. https://doi.org/10.29121/granthaalayah.v3.i12.2015.2882

Alsulaili, A. D., & Hamoda, M. F. (2015). Quantification and characterization of greywater from schools. *Water Science and Technology*, *72*(11), 1973–1980. https://doi.org/10.2166/wst.2015.408

Bear, J., & Cheng, A. (2010). Modeling Groundwater Flow and Contaminant Transport. In *Springer, Dordrecht* (Vol. 23). https://doi.org/10.1007/978-1-4020-6682-5

Bear, J., & Verruijt, A. (1987). The Finite Difference Method. In J. Bear & A. Verruijt (Eds.), *Modeling Groundwater Flow and Pollution* (pp. 225–246). Springer Netherlands. https://doi.org/10.1007/978-94-009-3379-8_9

Braddock, R. D., Parlange, J.-Y., & Lee, H. (2001). Application of a Soil Water Hysteresis Model to Simple Water Retention Curves. *Transport in Porous Media*, *44*(3), 407–420. https://doi.org/10.1023/A:1010792008870

Brooks, R. H., & Corey, A. T. (1964). Hydraulic Properties of Porous Media. *Hydrology Paper*, *7*, 26–28.

Brunetti, G., Papagrigoriou, I.-A., Šimůnek, J., & Stumpp, C. (2021). Green Roofs for domestic wastewater treatment: Experimental and numerical analysis of nitrogen turnover. *Journal of Hydrology*, *603*, 127132. https://doi.org/10.1016/j.jhydrol.2021.127132

Brutsaert, W. (2005). *Hydrology: An introduction*. Cambridge University Press.

Burszta-Adamiak, E., & Mrowiec, M. (2013). Modelling of Green roofs' hydrologic performance using EPA's SWMM. *Water Science and Technology : A Journal of the International Association on Water Pollution Research*, *68*, 36–42. https://doi.org/10.2166/wst.2013.219

Calvin, K., Dasgupta, D., Krinner, G., Mukherji, A., Thorne, P. W., Trisos, C., Romero, J., Aldunce, P., Barrett, K., Blanco, G., Cheung, W. W. L., Connors, S., Denton, F., Diongue-Niang, A., Dodman, D., Garschagen, M., Geden, O., Hayward, B., Jones, C., … Péan, C. (2023). *IPCC, 2023: Climate Change 2023: Synthesis Report.*

Contribution of Working Groups I, II and III to the Sixth Assessment Report of the Intergovernmental Panel on Climate Change [Core Writing Team, H. Lee and J. Romero (eds.)]. IPCC, Geneva, Switzerland. (First). Intergovernmental Panel on Climate Change (IPCC). https://doi.org/10.59327/IPCC/AR6-9789291691647

Chow, V., Maidment, D., & Mays, L. (1988). *Applied Hydrology*. *xiii*.

Chu, J., Chen, J., Wang, C., & Fu, P. (2004). Wastewater reuse potential analysis: Implications for China's water resources management. *Water Research*, *38*(11), 2746–2756. https://doi.org/10.1016/j.watres.2004.04.002

Cipolla, S. S., Maglionico, M., & Stojkov, I. (2016). A long-term hydrological modelling of an extensive green roof by means of SWMM. *Ecological Engineering*, *95*, 876–887. https://doi.org/10.1016/j.ecoleng.2016.07.009

Císlerová, M., & Vogel, T. (1998). *Transportní procesy*. https://katalog.vsb.cz/records/3eea936b-fef7-431b-91cf-fd2947d4731c?locale=cs

DeOreo, W. B., Mayer, P. W., Dziegielewski, B., & Kiefer, J. (2016). *Residential end uses of water, version 2*. Water Research Foundation. https://scholar.google.com/scholar?cluster=5211289153221218587&hl=en&oi=scholarr

Dusek, J., & Vogel, T. (2014). Modeling Subsurface Hillslope Runoff Dominated by Preferential Flow: One- vs. Two-Dimensional Approximation. *Vadose Zone Journal*, *13*(6), vzj2013.05.0082. https://doi.org/10.2136/vzj2013.05.0082

Farthing, M. W., & Ogden, F. L. (2017). Numerical Solution of Richards' Equation: A Review of Advances and Challenges. *Soil Science Society of America Journal*, *81*(6), 1257–1269. https://doi.org/10.2136/sssaj2017.02.0058

Friedler, E. (2004). Quality of Individual Domestic Greywater Streams and Its Implication on On-site Treatment and Reuse Possibilities. *Environmental Technology*, *25*, 997–1008. https://doi.org/10.1080/09593330.2004.9619393

Gajewska, M., Skrzypiec, K., Jóźwiakowski, K., Mucha, Z., Wójcik, W., Karczmarczyk, A., & Bugajski, P. (2020). Kinetics of pollutants removal in vertical and horizontal flow constructed wetlands in temperate climate. *Science of The Total Environment, 718*, 137371. https://doi.org/10.1016/j.scitotenv.2020.137371

Gärdenäs, A. I., Hopmans, J. W., Hanson, B. R., & Šimůnek, J. (2005). Two-dimensional modeling of nitrate leaching for various fertigation scenarios under micro-irrigation. *Agricultural Water Management, 74*(3), 219–242. https://doi.org/10.1016/j.agwat.2004.11.011

Getter, K., & Rowe, D. (2006). The Role of Extensive Green Roofs in Sustainable Development. *HortScience: A Publication of the American Society for Horticultural Science*, *41*, 1276. https://doi.org/10.21273/HORTSCI.41.5.1276

Ghermandi, A. (2005). *Evaluating functions and benefits of constructed wetlands*. https://www.semanticscholar.org/paper/Evaluating-functions-and-benefits-of-constructed-Ghermandi/dc2e23ab817a06a489d15d090f7161e3f036dff2

Gross, A., Azulai, N., Oron, G., Ronen, Z., Arnold, M., & Nejidat, A. (2005). Environmental impact and health risks associated with greywater irrigation: A case study. *Water Science and Technology : A Journal of the International Association on Water Pollution Research*, *52*, 161–169. https://doi.org/10.2166/wst.2005.0251

Hillel, D. (2003). *Introduction to Environmental Soil Physics* (p. 494).

Hilten, R., Lawrence, T., & Tollner, E. (2008). Modeling stormwater runoff from green roofs with HYDRUS-1D. *Journal of Hydrology - J HYDROL*, *358*, 288–293. https://doi.org/10.1016/j.jhydrol.2008.06.010

Horton, R. (1933). The Role of Infiltration in the Hydrologic Cycle. *Trans. Am. Geophys. Union*, *14*, 446. https://doi.org/10.1029/TR014i001p00446

Kadlec, R., Knight, R., Vymazal, J., Brix, H., Cooper, P., & Haberl, R. (2000). *Constructed Wetlands for Pollution Control: Processes, Performance, Design and Operation* (p. 156).

Knapp, S., Schmauck, S., & Zehnsdorf, A. (2019). Biodiversity Impact of Green Roofs and Constructed Wetlands as Progressive Eco-Technologies in Urban Areas. *Sustainability*, *11*(20), Article 20. https://doi.org/10.3390/su11205846

Kollet, S. J., & Maxwell, R. M. (2006). Integrated surface–groundwater flow modeling: A free-surface overland flow boundary condition in a parallel groundwater flow model. *Advances in Water Resources*, *29*(7), 945–958. https://doi.org/10.1016/j.advwatres.2005.08.006

Langergraber, G., & Šimůnek, J. (2012). Reactive Transport Modeling of Subsurface Flow Constructed Wetlands Using the HYDRUS Wetland Module. *Vadose Zone Journal*, *11*(2), vzj2011.0104. https://doi.org/10.2136/vzj2011.0104

Lata, J.-C., Dusza, Y., Abbadie, L., Barot, S., Carmignac, D., Gendreau, E., Kraepiel, Y., Mériguet, J., Motard, E., & Raynaud, X. (2018). Role of substrate properties in the provision of multifunctional green roof ecosystem services. *Applied Soil Ecology*, *123*, 464–468. https://doi.org/10.1016/j.apsoil.2017.09.012

Li, Y., & Babcock, R. W. (2014). Green roofs against pollution and climate change. A review. *Agronomy for Sustainable Development*, *34*(4), 695–705. https://doi.org/10.1007/s13593-014-0230-9

Liu, J., Yang, H., Gosling, S. N., Kummu, M., Flörke, M., Pfister, S., Hanasaki, N., Wada, Y., Zhang, X., Zheng, C., Alcamo, J., & Oki, T. (2017). Water scarcity assessments in the past, present, and future. *Earth's Future*, *5*(6), 545–559. https://doi.org/10.1002/2016EF000518

Maimon, A., Tal, A., Friedler, E., & Gross, A. (2010). Safe on-Site Reuse of Greywater for Irrigation—A Critical Review of Current Guidelines. *Environmental Science & Technology*, *44*(9), 3213–3220. https://doi.org/10.1021/es902646g

Mašková, A. (2022). *Design and testing of the flume for a hybrid wetland-extensive green roof*. Czech Technical University in Prague.

Masrouri, F., Bicalho, K., & Kawai, K. (2008). Laboratory Hydraulic Testing in Unsaturated Soils. *Laboratory and Field Testing of Unsaturated Soils*, *26*, 691–704. https://doi.org/10.1007/s10706-008-9202-7

Moslemi Zadeh, S., Hunt, D., Lombardi, D., & Rogers, C. (2013). Shared Urban Greywater Recycling Systems: Water Resource Savings and Economic Investment. *Sustainability*, *5*, 2887–2912. https://doi.org/10.3390/su5072887

Niazi, M., Nietch, C., Maghrebi, M., Jackson, N., Bennett, B. R., Tryby, M., & Massoudieh, A. (2017). Storm Water Management Model: Performance Review and Gap Analysis. *Journal of Sustainable Water in the Built Environment*, *3*(2), 04017002. https://doi.org/10.1061/JSWBAY.0000817

nimmo, john, & Landa, E. (2005). *The Soil Physics Contributions of Edgar Buckingham*. Soil Science Society of America Journal - Wiley Online Library. https://acsess.onlinelibrary.wiley.com/doi/10.2136/sssaj2005.0328

Oberndorfer, E., Lundholm, J., Bass, B., Coffman, R. R., Doshi, H., Dunnett, N., Gaffin, S., Köhler, M., Liu, K. K. Y., & Rowe, B. (2007). Green Roofs as Urban Ecosystems: Ecological Structures, Functions, and Services. *BioScience*, *57*(10), 823–833. https://doi.org/10.1641/B571005

Oteng-Peprah, M., Acheampong, M. A., & deVries, N. K. (2018). Greywater Characteristics, Treatment Systems, Reuse Strategies and User Perception—A Review. *Water, Air, & Soil Pollution*, *229*(8), 255. https://doi.org/10.1007/s11270-018-3909-8

Petreje, M., Sněhota, M., Chorazy, T., Novotný, M., Rybová, B., & Hečková, P. (2023). Performance study of an innovative concept of hybrid constructed wetland-extensive

green roof with growing media amended with recycled materials. *Journal of Environmental Management*, *331*, 117151. https://doi.org/10.1016/j.jenvman.2022.117151

Pucher, B., & Langergraber, G. (2018). Simulating vertical flow wetlands using filter media with different grain sizes with the HYDRUS Wetland Module. *Journal of Hydrology and Hydromechanics*, *66*(2), 227–231. https://doi.org/10.1515/johh-2017-0053

Revitt, D. M., Eriksson, E., & Donner, E. (2011). The implications of household greywater treatment and reuse for municipal wastewater flows and micropollutant loads. *Water Research*, *45*(4), 1549–1560. https://doi.org/10.1016/j.watres.2010.11.027

Šálek, J., Kriška, M., Pírek, O., Plotěný, K., Rozkošný, M., & Žáková, Z. (2013, June 20). Vegetační Kořenové Čistírny. *Tbz-Info*. https://m.tzb-info.cz/likvidace-odpadnich-vod/10058-vegetacni-korenove-cistirny#:~:text=Kořenová%20čist%C3%ADrna%20je%20vhodná%20zejména,z%20jednotné%20kanalizace.

Shahsavani, E., Ehrampoush, M., Samaei, M., Mehrizi, E., Madadizadeh, F., Abbasi, A., Shiranian, M., Mohammadpour, A., & Ebrahimi, A. (2022). Real and Synthetic Greywater Treatment by a Combined Process of Ozonation, Granular Activated Carbon, and Ultrafiltration. *Health Scope*, *11*. https://doi.org/10.5812/jhealthscope-123644

Shaikh, I. N., & Ahammed, M. M. (2020). Quantity and quality characteristics of greywater: A review. *Journal of Environmental Management*, *261*, 110266. https://doi.org/10.1016/j.jenvman.2020.110266

Shuval, H., Lampert, Y., & Fattal, B. (1997). Development of a risk assessment approach for evaluating wastewater reuse standards for agriculture. *Water Science and Technology*, *35*(11–12), 15–20. https://doi.org/10.2166/wst.1997.0703

Šimůnek, J., van Genuchten, M. Th., & Šejna, M. (2016). Recent Developments and Applications of the HYDRUS Computer Software Packages. *Vadose Zone Journal*, *15*(7), vzj2016.04.0033. https://doi.org/10.2136/vzj2016.04.0033

Sposito, G., Gupta, V., & Bhattacharya, R. (1979). Foundation theories of solute transport in porous media: A critical review. *Advances in Water Resources*, *2*, 59–68. https://doi.org/10.1016/0309-1708(79)90012-5

Stefanakis, A. (2016). *Constructed Wetlands: Description and Benefits of an Eco-Tech Water Treatment System* (pp. 281–303). https://doi.org/10.4018/978-1-4666-9559-7.ch012

Stefanakis, A. I. (2019). The Role of Constructed Wetlands as Green Infrastructure for Sustainable Urban Water Management. *Sustainability*, *11*(24), Article 24. https://doi.org/10.3390/su11246981

van Genuchten, M. Th. (1980). A Closed-form Equation for Predicting the Hydraulic Conductivity of Unsaturated Soils. *Soil Science Society of America Journal*, *44*(5), 892–898. https://doi.org/10.2136/sssaj1980.03615995004400050002x

Vogel, T. (1987). SWMII - Numerical model of two-dimensional flow in a variably saturated porous medium. In *Research report nr. 87. Vakgroep Hydraulica en Afvoerhydrologie. LUW (1988) 120 pp.*

Vogel, T., Gerke, H. H., Zhang, R., & Van Genuchten, M. Th. (2000). Modeling flow and transport in a two-dimensional dual-permeability system with spatially variable hydraulic properties. *Journal of Hydrology*, *238*(1), 78–89. https://doi.org/10.1016/S0022-1694(00)00327-9

Vymazal, J. (2007). Removal of nutrients in various types of constructed wetlands. *Science of The Total Environment*, *380*(1–3), 48–65. https://doi.org/10.1016/j.scitotenv.2006.09.014

Wang, X., Tian, Y., & Zhao, X. (2017). The influence of dual-substrate-layer extensive green roofs on rainwater runoff quantity and quality. *Science of The Total Environment*, *592*, 465–476. https://doi.org/10.1016/j.scitotenv.2017.03.124

Zotarelli, L., Dukes, M. D., Romero, C. C., Migliaccio, K. W., & Morgan, K. T. (2010). Step by step calculation of the Penman-Monteith Evapotranspiration (FAO-56 Method). *Institute of Food and Agricultural Sciences. University of Florida*, *8*. http://www.agraria.unirc.it/documentazione/materiale_didattico/1462_2016_412_24509.pdf

Food and Agriculture Organization of the United Nations. (1998). *Crop evapotranspiration: Guidelines for computing crop water requirements* (FAO Irrigation and Drainage Paper 56, Chapter 6). Rome: FAO. Retrieved May 14, 2024

LIST OF TABLES

LIST OF FIGURES

Appendix

Table 10 Time Variable Boundary conditions in HYDRUS 2D model

Time	rainfall	evaporation	transpiration	hCritA	Var.Fl. 1	cValue2
[hr]	[cm/hr]	[cm/hr]	[cm/hr]	[cm]	[cm/hr]	[mg/cm3]
0.0083	0	0.008089	0	10000	-1206.8	0.02
0.0167	0	0.008089	0	10000	-1206.8	0.02
0.0194	0	0.008089	0	10000	-778.56	0.02
0.0208	0	0.008089	0	10000	-467.13	0.02
0.0222	0	0.008089	0	10000	-155.71	0.02
0.0236	0	0.008089	0	10000	-62.284	0.02
0.03	0	0.008089	0	10000	0	0.00
24	0	0.006931	0	10000	0	0.00
24.004	0	0.006931	0	10000	-1786.2	0.02
24.008	0	0.006931	0	10000	-3572.3	0.02
24.012	0	0.006931	0	10000	-1786.2	0.02
24.017	0	0.006931	0	10000	0	0.00
25	0	0.006931	0	10000	0	0.00
48	0	0.0085	0	10000	0	0.00
48.004	0	0.0085	0	10000	-1829.2	0.02
48.008	0	0.0085	0	10000	-3658.5	0.02
48.012	0	0.0085	0	10000	-1829.2	0.02
48.017	0	0.0085	0	10000	0	0.00
49	0	0.0085	0	10000	0	0.00
72	0	0.009063	0	10000	0	0.00
72.004	0	0.009063	0	10000	-1772.5	0.02
72.008	0	0.009063	0	10000	-3545	0.02
72.012	0	0.009063	0	10000	-1772.5	0.02
72.017	0	0.009063	0	10000	0	0.00
73	0	0.010571	0	10000	0	0.00
96	0	0.010571	0	10000	0	0.00
96.004	0	0.010571	0	10000	-1681.4	0.02
96.008	0	0.010571	0	10000	-3362.9	0.02
96.012	0	0.010571	0	10000	-1681.4	0.02
96.017	0	0.010571	0	10000	0	0.00
97	0	0.010571	0	10000	0	0.00
120	0	0.007585	0	10000	0	0.00
120	0	0.007585	0	10000	-1518.9	0.02
120.01	0	0.007585	0	10000	-3037.8	0.02

120.01	0	0.007585	0	10000	-1518.9	0.02
120.02	0	0.007585	0	10000	0	0.00
121	0	0.007585	0	10000	0	0.00
129.43	0	0.007585	0	10000	0	0.00
129.53	0.2	0.007585	0	10000	0	0.00
129.65	0.1714	0.007585	0	10000	0	0.00
130.05	0.05	0.007585	0	10000	0	0.00
141	0	0.007941	0	10000	0	0.00
144	0	0.007941	0	10000	0	0.00
144	0	0.007941	0	10000	-1688.4	0.02
144.01	0	0.007941	0	10000	-3376.9	0.02
144.01	0	0.007941	0	10000	-1688.4	0.02
144.02	0	0.007941	0	10000	0	0.00
145	0	0.007941	0	10000	0	0.00
164	0	0.007941	0	10000	0	0.00
164.68	1.2	0.001294	0	10000	0	0.00
164.75	0.3	0.001294	0	10000	0	0.00
164.81	1.2	0.001294	0	10000	0	0.00
164.85	0.6	0.001294	0	10000	0	0.00
164.86	1.2	0.001294	0	10000	0	0.00
164.9	0.6	0.001294	0	10000	0	0.00
165.03	0.15	0.001294	0	10000	0	0.00
165.1	0.3	0.001294	0	10000	0	0.00
165.18	0.24	0.001294	0	10000	0	0.00
165.37	0.1091	0.001294	0	10000	0	0.00
165.43	0.3	0.001294	0	10000	0	0.00
165.48	0.4	0.001294	0	10000	0	0.00
165.63	0.1333	0.001294	0	10000	0	0.00
165.82	0.1091	0.001294	0	10000	0	0.00
165.98	0.12	0.001294	0	10000	0	0.00
166.05	0.3	0.001294	0	10000	0	0.00
166.32	0.15	0.001294	0	10000	0	0.00
166.52	0.1	0.001294	0	10000	0	0.00
166.6	0.24	0.001294	0	10000	0	0.00
166.65	0.4	0.001294	0	10000	0	0.00
166.77	0.3	0.001294	0	10000	0	0.00
166.85	0.24	0.001294	0	10000	0	0.00
166.92	0.3	0.001294	0	10000	0	0.00
167	0.24	0.001294	0	10000	0	0.00

167.15	0.3	0.001294	0	10000	0	0.00
167.23	0.24	0.001294	0	10000	0	0.00
167.3	0.3	0.001294	0	10000	0	0.00
167.35	0.4	0.001294	0	10000	0	0.00
167.42	0.3	0.001294	0	10000	0	0.00
167.47	0.4	0.001294	0	10000	0	0.00
167.5	0.3	0.001294	0	10000	0	0.00
167.53	0	0.001294	0	10000	0	0.00
167.62	0.24	0.001294	0	10000	0	0.00
167.8	0.2	0.001294	0	10000	0	0.00
167.88	0.24	0.001294	0	10000	0	0.00
167.98	0.2	0.001294	0	10000	0	0.00
168	0.1333	0.001294	0	10000	0	0.00
168	0.1333	0.001294	0	10000	-1708.1	0.02
168.01	0.1333	0.001294	0	10000	-3416.1	0.02
168.01	0.1333	0.001294	0	10000	-1708.1	0.02
168.02	0.1333	0.001294	0	10000	0	0.00
168.05	0.1333	0.001294	0	10000	0	0.00
168.27	0.15	0.001294	0	10000	0	0.00
168.52	0.08	0.001294	0	10000	0	0.00
168.72	0.1	0.001294	0	10000	0	0.00
169.03	0.1714	0.001294	0	10000	0	0.00
169.27	0.0857	0.001294	0	10000	0	0.00
169.53	0.075	0.001294	0	10000	0	0.00
169.9	0.0545	0.001294	0	10000	0	0.00
170.05	0.1333	0.001294	0	10000	0	0.00
172.78	0.0073	0.001294	0	10000	0	0.00
174.53	0.0114	0.001294	0	10000	0	0.00
180.65	0.0033	0.001294	0	10000	0	0.00
180.92	0.075	0.001294	0	10000	0	0.00
181.13	0.0923	0.001294	0	10000	0	0.00
181.4	0.075	0.001294	0	10000	0	0.00
181.53	0.15	0.001294	0	10000	0	0.00
181.62	0.24	0.001294	0	10000	0	0.00
181.72	0.2	0.001294	0	10000	0	0.00
181.8	0.24	0.001294	0	10000	0	0.00
181.93	0.4	0.001294	0	10000	0	0.00
182	0.3	0.002078	0	10000	0	0.00
182.05	0.4	0.002078	0	10000	0	0.00

182.13	0.24	0.002078	0	10000	0	0.00
182.22	0.24	0.002078	0	10000	0	0.00
182.28	0.3	0.002078	0	10000	0	0.00
182.37	0.24	0.002078	0	10000	0	0.00
182.5	0.15	0.002078	0	10000	0	0.00
183.45	0.0211	0.002078	0	10000	0	0.00
185.57	0.0094	0.002078	0	10000	0	0.00
185.95	0.0522	0.002078	0	10000	0	0.00
186.23	0.0706	0.002078	0	10000	0	0.00
186.38	0.1333	0.002078	0	10000	0	0.00
186.45	0.3	0.002078	0	10000	0	0.00
186.53	0.24	0.002078	0	10000	0	0.00
186.67	0.15	0.002078	0	10000	0	0.00
186.83	0.12	0.002078	0	10000	0	0.00
187.17	0.06	0.002078	0	10000	0	0.00
187.28	0.1714	0.002078	0	10000	0	0.00
187.42	0.15	0.002078	0	10000	0	0.00
187.63	0.24	0.002078	0	10000	0	0.00
187.7	0.3	0.002078	0	10000	0	0.00
187.83	0.15	0.002078	0	10000	0	0.00
187.98	0.1333	0.002078	0	10000	0	0.00
188.12	0.15	0.002078	0	10000	0	0.00
188.2	0.24	0.002078	0	10000	0	0.00
188.33	0.15	0.002078	0	10000	0	0.00
188.4	0.3	0.002078	0	10000	0	0.00
188.58	0.4	0.002078	0	10000	0	0.00
188.67	0.6	0.002078	0	10000	0	0.00
188.72	0.4	0.002078	0	10000	0	0.00
188.8	0.6	0.002078	0	10000	0	0.00
188.88	0.4	0.002078	0	10000	0	0.00
188.92	0.6	0.002078	0	10000	0	0.00
188.97	0.4	0.002078	0	10000	0	0.00
189.07	0.2	0.002078	0	10000	0	0.00
189.13	0.3	0.002078	0	10000	0	0.00
189.23	0.2	0.002078	0	10000	0	0.00
189.43	0.1	0.002078	0	10000	0	0.00
191.43	0.01	0.002078	0	10000	0	0.00
191.58	0.1333	0.002078	0	10000	0	0.00
191.75	0.12	0.002078	0	10000	0	0.00

192	0.0279	0.002078	0	10000	0	0.00
192	0.0279	0.002078	0	10000	-1912.5	0.02
192.01	0.0279	0.002078	0	10000	-3825	0.02
192.01	0.0279	0.002078	0	10000	-1912.5	0.02
192.02	0.0279	0.002078	0	10000	0	0.00
193	0	0.002471	0	10000	0	0.00
216	0	0.002471	0	10000	0	0.00
216	0	0.002471	0	10000	-2079.5	0.02
216.01	0	0.002471	0	10000	-4159	0.02
216.01	0	0.002471	0	10000	-2079.5	0.02
216.02	0	0.002471	0	10000	0	0.00
234.5	0	0.000697	0	10000	0	0.00
234.58	0.24	0.000697	0	10000	0	0.00
234.68	0.2	0.000697	0	10000	0	0.00
234.75	0.3	0.000697	0	10000	0	0.00
234.83	0.24	0.000697	0	10000	0	0.00
235.02	0.1091	0.000697	0	10000	0	0.00
235.25	0.0857	0.000697	0	10000	0	0.00
235.62	0.0545	0.000697	0	10000	0	0.00
235.78	0.12	0.000697	0	10000	0	0.00
236.05	0.075	0.000697	0	10000	0	0.00
236.18	0.15	0.000697	0	10000	0	0.00
236.35	0.12	0.000697	0	10000	0	0.00
236.48	0.15	0.000697	0	10000	0	0.00
236.58	0.2	0.000697	0	10000	0	0.00
236.72	0.3	0.000697	0	10000	0	0.00
236.87	0.3	0.000697	0	10000	0	0.00
236.93	0.3	0.000697	0	10000	0	0.00
237	0.24	0.000697	0	10000	0	0.00
237.02	0	0.000697	0	10000	0	0.00
237.17	0.4	0.000697	0	10000	0	0.00
237.28	0.1714	0.000697	0	10000	0	0.00
237.67	0.2	0.000697	0	10000	0	0.00
237.82	0.1333	0.000697	0	10000	0	0.00
238	0.0316	0.000697	0	10000	0	0.00
239.12	0.1714	0.000697	0	10000	0	0.00
239.18	0.3	0.000697	0	10000	0	0.00
239.27	0.24	0.000697	0	10000	0	0.00
239.38	0.1714	0.000697	0	10000	0	0.00

239.47	0.24	0.000697	0	10000	0	0.00
239.57	0.2	0.000697	0	10000	0	0.00
239.9	0.2	0.000697	0	10000	0	0.00
240	0.0094	0.000697	0	10000	0	0.00
240	0.0094	0.000697	0	10000	-2066.3	0.02
240.01	0.0094	0.000697	0	10000	-4132.7	0.02
240.01	0.0094	0.000697	0	10000	-2066.3	0.02
240.02	0.0094	0.000697	0	10000	0	0.00
240.05	0.0094	0.000697	0	10000	0	0.00
242.03	0.0571	0.000697	0	10000	0	0.00
242.3	0.075	0.000697	0	10000	0	0.00
242.53	0.0857	0.000697	0	10000	0	0.00
242.62	0.24	0.000697	0	10000	0	0.00
242.65	0.6	0.000697	0	10000	0	0.00
242.72	0.3	0.000697	0	10000	0	0.00
243.03	0.0632	0.000697	0	10000	0	0.00
243.75	0.0279	0.000697	0	10000	0	0.00
243.92	0.12	0.000697	0	10000	0	0.00
244.12	0.1	0.000697	0	10000	0	0.00
244.25	0.15	0.000697	0	10000	0	0.00
245.63	0.0145	0.000697	0	10000	0	0.00
246.65	0.0197	0.000697	0	10000	0	0.00
247.75	0.0182	0.000697	0	10000	0	0.00
249.37	0.0124	0.000697	0	10000	0	0.00
263	0	0.000697	0	10000	0	0.00
264	0	0.000697	0	10000	0	0.00